CMS TN/94-285
December 28, 1994

CMS Level 1 Calorimeter Trigger Performance Studies

S. Dasu, J. Lackey, W. H. Smith, W. Temple
Physics Department, University of Wisconsin
Madison WI 53706

Abstract

The level 1 calorimeter trigger system for the CMS detector at the LHC collider must provide a deadtimeless, pipelined trigger that implements simple algorithms which satisfy the physics efficiency and data rate requirements. In this note we examine the performance of a conceptual design and that of an alternate algorithm for the electron trigger. The algorithms account for energy sharing between neighboring towers and perform hadronic, and optionally, electromagnetic isolation. Through extensive simulation of the level 1 calorimeter trigger, we have determined the background rates and efficiencies of triggers for electrons, photons and jets.

1 Introduction

We present simulation results for a conceptual design [1] of a level 1 calorimeter trigger system for the CMS detector [2]. For the nominal LHC design luminosity of $10^{34}\mathrm{cm}^{-2}\mathrm{s}^{-1}$, several tens of events occur at the beam crossing frequency of 40 MHz. This input rate of 10^9 interactions every second must be reduced by a factor of at least 10^7 to 100 Hz, the maximum rate that can be archived by the on-line computer farm. CMS has chosen to reduce this rate in two steps. The first level stores all data for 3 μs, after which no more than a 100 kHz rate of the stored events is forwarded to the higher level triggers. This must be done for all channels without dead time. A second level of trigger is provided by a subset of the on-line processor farm, which passes a fraction of these events for further filtering by the remainder of the on-line farm. During the 3 μs of the level 1 trigger processing time, trigger decisions must be developed that discard a large fraction of the data while retaining the small portion coming from interactions of interest.

The physics requirements on the level 1 calorimeter trigger are:

- The CMS trigger system should be capable of selecting leptons and jets over the pseudorapidity range $|\eta| < 2.6$, with an efficiency which is very high above a selected threshold[1] in transverse momentum.
- For the single lepton triggers it is required that the trigger is fully efficient (> 95%) in the pseudorapidity range $|\eta| < 2.5$, with a threshold of $p_t > 40$ GeV/c.
- For the dilepton trigger, it is required that the trigger is fully efficient (> 95%) in the pseudorapidity range $|\eta| < 2.5$ with a threshold of $p_t > 20$ GeV/c for each lepton.
- Single photon and diphoton triggers are required to have thresholds similar to those of the leptons.
- Single and multiple jet triggers are required with a well defined efficiency in order to reconstruct jet spectra that overlap with data attainable at lower energy colliders such as the Tevatron. For higher transverse momenta the jet trigger should also be fully efficient.
- A missing transverse energy trigger with a threshold of about 100 GeV is required.

The hard scattering physics to be studied at the LHC includes signals such as Higgs decays to two photons or four leptons, W-W scattering, supersymmetry, Z′ and top decays. Many of these processes involve W decays. Due to the low mass of the W compared to the energies at the LHC, the tightest constraint on a single electron trigger comes from a requirement to trigger on W decays. Therefore, to be able to trigger on hard scattering physics signals, we have set up a requirement, as a benchmark, that the level 1 calorimeter isolated electron

[1] In this paper we use "p_t threshold" to identify the 95% efficiency point and "E_t cutoff" to specify the cut off value programmed in the trigger.

trigger provide about 50% efficiency for identifying W decay electrons (integrated over all electron momenta). This results in a single isolated electron trigger p_t threshold of about 40 GeV. The Higgs (80 GeV mass) decay to two photons with $> 95\%$ efficiency determines the requirement for the isolated double photon trigger to have about a 20 GeV p_t threshold. Note that these level 1 p_t thresholds are, and ought to be, somewhat smaller than the offline physics analysis cuts. The reason for such a requirement is that the efficiency turn-on curves for the level 1 trigger will be somewhat softer than can be achieved with a full analysis including the best resolutions and calibration corrections.

We must also plan for the evolution in the physics processes studied as the LHC luminosity increases from about 10^{32} to 10^{34} cm^{-2} s^{-1}. Lower p_t thresholds and removal or relaxation of isolation cuts will be useful to maximize the physics output during lower luminosity and also to match with the Tevatron data.

The uncertainties in estimates of cross sections at high energies and limited knowledge of branching ratios impose a large error on the estimated trigger rates. In addition we cannot assume that the CMS DAQ system will always run at its maximum design capacity. Therefore, we provide for a safety margin of a factor of three from the design 100 kHz maximum level 1 output rate to 30 kHz, in designing algorithms for level 1 triggers. Furthermore, this 30 kHz bandwidth of level 1 output has to be shared amongst several triggers such as those for single and double electrons/photons, jets, missing energy, tau and single and double muons. Therefore, target for the individual trigger rates is a few kHz.

All initial trigger decisions are based on local information, rather than on global event topology. The level 1 trigger processors work by selecting events based on single particles or jets. The dilepton, diphoton and other combination triggers are achieved by a global processor which counts the numbers of individual triggers. Some coarse correlation in the object positions is also possible. It is important to remember that the input data bandwidth and trigger processing time considerably limit the information from the muon and calorimeter systems that is available for trigger calculations.

The level 1 trigger for electrons, photons, jets and neutrinos is primarily based on the calorimeter. In order to establish the requirements, specify algorithms for the level 1 trigger, and evaluate trigger hardware design, several Monte Carlo studies using a parametric response of the calorimeter were done. The results from these studies are described below.

2 Calorimeter Trigger Algorithms

2.1 Input Data

The calorimeter level 1 trigger system receives digital trigger sums on an eight bit compressed scale. Programmable tables will enable full flexibility to modify the compression algorithm as required. The trigger system will use memory lookup tables to decode the 8-bit compressed scale data into a linear scale with a 10 bit dynamic range in the adder tree.

Our proposed mapping of physical calorimeter towers into trigger towers is discussed in detail in section 3. There is a 1:1 correspondence between the HCAL and ECAL trigger

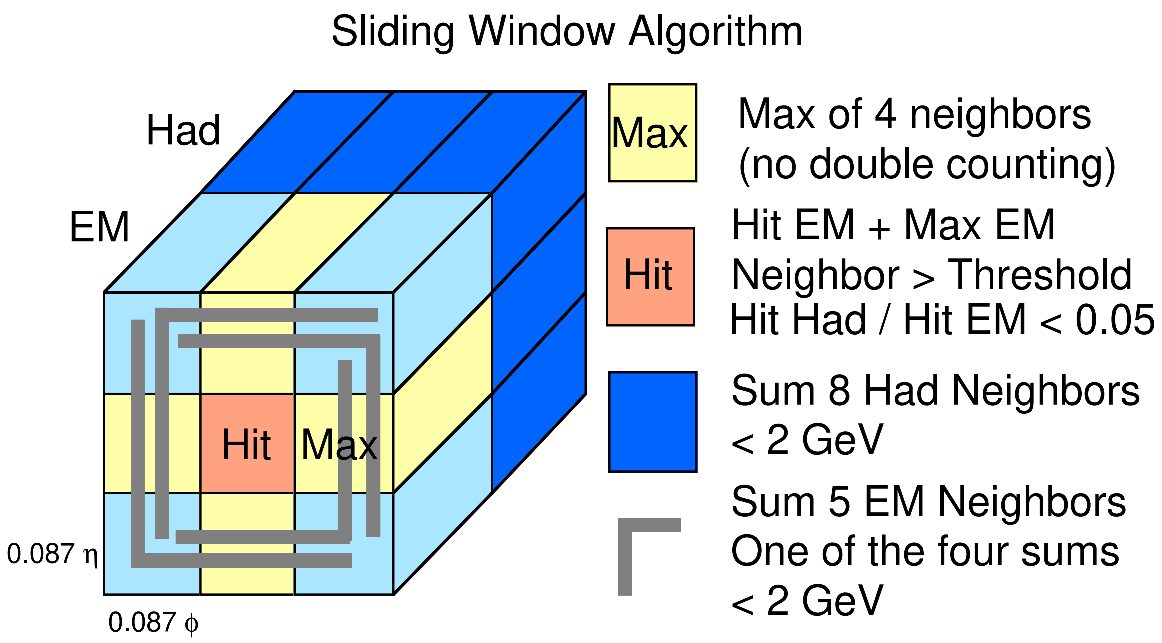

Figure 1: Sliding window electron trigger algorithm.

towers. The trigger tower size is equivalent to the HCAL physical towers, $.0873 \times .0873$ in $\eta \times \phi$. The ϕ size remains constant in $\Delta\phi$ and the η size remains constant in $\Delta\eta$ down to an η of 2.1, beyond which the η size doubles. There are 3888 total ECAL and 3888 total HCAL trigger towers from η = -2.6 to η = 2.6 (54 x 72 $\eta - \phi$ divisions).

2.2 "Sliding Window" Algorithm

Figure 1 shows our preferred proposal for an electron/photon trigger algorithm. This "sliding window" algorithm considers all 3x3 trigger tower regions centered on every trigger tower in the system. The ECAL transverse energy sum of the central trigger tower with the maximum of the four neighbors within the 3x3 window is checked against various E_t cutoffs. The addition of the energy in the neighboring tower ensures that any leakage out of the primary tower is included. This results in a sharper efficiency curve turn-on. The algorithm then involves two separate cuts on the longitudinal and transverse isolation of the HAD energy deposit to reduce the background rate from QCD jet events. The first cut involves the hit tower HAD to EM energy ratio ($H/E < 0.05$). A second cut requires HAD transverse isolation, i.e. a cut on the sum of HAD transverse energies in the nearest eight towers surrounding the hit tower ($\Sigma_8 H < 2$ GeV).

The isolation on hadronic towers can be very tight because we expect very little leakage

8 bit value	Transverse Energy
0, 1, ... 63,	0., 0.1, ... 6.3
64, 65, ... 127,	6.8, 7.3, ... 38.3
128, 129, ... 191,	39.3, 40.3, ... 102.3
192, 193, ... 254,	104.3, 106.3, ... 228.3
255	$\geq$ 230.3

Table 1: Example of 8-bit quadlinear scale for trigger data transmission.

of the electron/photon shower energy into the hadronic section of the calorimeter. The separation of longitudinal and transverse isolation is done so that at lower luminosities one can use only longitudinal isolation to trigger on events with electrons close to jets, such as those due to semileptonic decays of heavy quarks. The HAD transverse isolation provides additional suppression of jet events in the electron trigger at higher luminosities by cutting on any energy deposited in the HCAL section by charged pions. An optional ECAL transverse isolation of the electron/photon energy deposit is also considered in this simulation to reduce the background further by cutting on energy deposited in the ECAL section by photons in jets. The EM isolation is provided by considering all four 5-tower corners of the 3x3 window (see Figure 1) and requiring that at least one of them is below a cutoff ($\Sigma_5 E < 2$ GeV). The act of checking all four 5-tower corners ensures that the candidates depositing energy in any corner of the central tower do not self-veto due to leakage energy, and it avoids the problem of determining which of the four combinations to pick.

2.3 Energy Scale

The trigger data needs to be limited to eight bits of transverse energy for both ECAL and HCAL towers in order to reduce both bandwidth and trigger logic hardware. For achieving the best dynamic dynamic range and resolution using these eight bit data we propose to use a quadlinear scale such as that shown in Table 1. This scale provides the high resolution needed for providing tight cuts on transverse isolation for the electron trigger and large dynamic range for high thresholds for the jet trigger. The quadlinear data is linearized in memory lookups in the trigger system to provide a 0.5 GeV 8-bit energy scale for the electron/photon trigger and 1 GeV 8-bit energy scale for the jet trigger. All energies in the trigger system are set so that, when the scale overflows, the energy is set to the maximum value allowed.

In order to implement the "sliding window" algorithm, data is required from one ring of the nearest neighbor towers for each reference tower. This requires that data be shared across trigger cards as well as crates [1]. However, only the lower 2 bits of neighboring HCAL tower information is sufficient because the HCAL neighbor tower information is only used to place a tight cut (≈ 2 GeV), and is used only for relatively lower momentum electron/photon

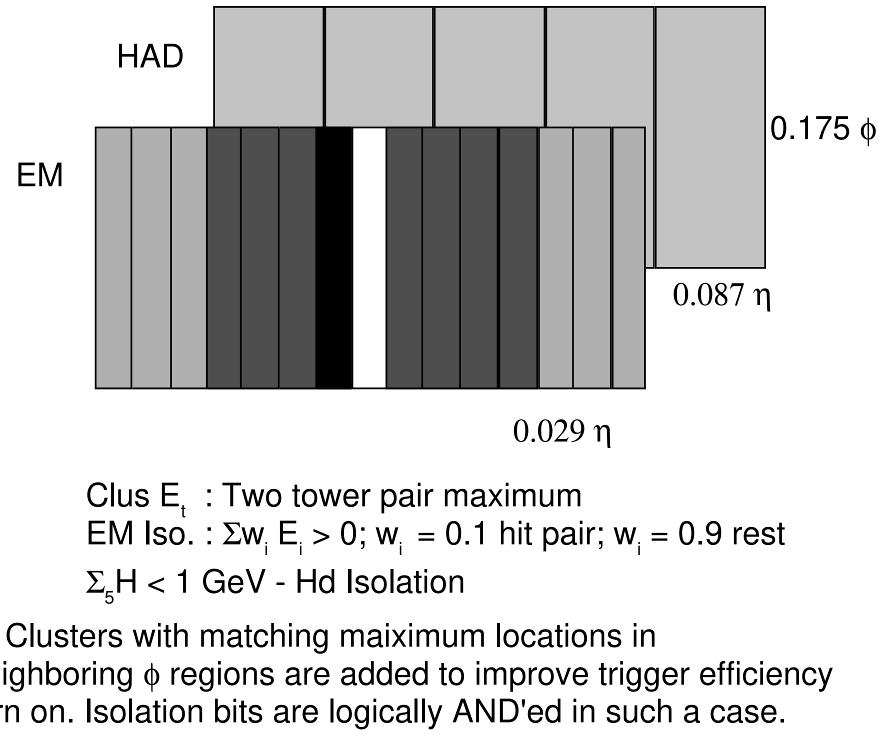

Figure 2: Peak finding electron trigger algorithm.

candidates. We have also limited the neighboring ECAL tower information to 6 bits when the data needs to go over the backplane. Furthermore, the look-up-table which contains the programmed values for H/E cut uses the bottom 4 bits of HCAL and top 4 bits of ECAL transverse energies only. All these limitations have been determined to cause only negligible degradation of the performance of the trigger. In the following results for the "sliding window" trigger we use these limited transverse energy scales.

2.4 "Peak-Finding" Algorithm

An alternate proposal for the electron/photon trigger, called the "peak finding" algorithm [3, 4] and adapted to the trigger tower geometry as described below, is also simulated. This algorithm considers rectangular trigger towers in the region shown in Figure 2. The central nine EM towers are scanned over the entire range of the calorimeter to provide a trigger over for the full range, i.e, $|\eta| < 2.6$. The three EM trigger tower side bands and the HAD trigger towers are used to provide isolation. Pairs of EM trigger towers are formed by combining each of the central nine towers with the tower to its right. The ECAL cluster E_t is defined as the maximum of these nine two-tower pairs. The algorithm then applies two isolation cuts. In the first, the ratio of the cluster transverse energy to the total ECAL transverse energy in the 15 EM tower region is required to be higher that 0.9. In the second, the hadronic

Calorimeter Section	Calorimeter Granularity	Trigger Granularity	
		Sliding Window	Peak finding
ECAL $-1.566 < \eta < 1.566$	$360\phi \times 216\eta$	$72\phi \times 36\eta$	$36\phi \times 108\eta$
ECAL $1.566 < \lvert\eta\rvert < 1.653$	$72\phi \times 2\eta$	$72\phi \times 2\eta$	$36\phi \times 2\eta$
ECAL $1.653 < \lvert\eta\rvert < 2.001$	$288\phi \times 32\eta$	$72\phi \times 8\eta$	$36\phi \times 16\eta$
ECAL $2.001 < \lvert\eta\rvert < 2.088$	$216\phi \times 6\eta$	$72\phi \times 2\eta$	
ECAL $2.088 < \lvert\eta\rvert < 2.349$	$216\phi \times 18\eta$	$72\phi \times 3\eta$	
ECAL $2.001 < \lvert\eta\rvert < 2.349$	$216\phi \times 24\eta$		$36\phi \times 12\eta$
ECAL $2.349 < \lvert\eta\rvert < 2.610$	$144\phi \times 12\eta$	$72\phi \times 3\eta$	$36\phi \times 6\eta$
HCAL $-2.088 < \eta < 2.088$	$72\phi \times 48\eta$	$72\phi \times 48\eta$	
HCAL $2.088 < \lvert\eta\rvert < 2.61$	$72\phi \times 6\eta$	$72\phi \times 6\eta$	
HCAL $-1.653 < \eta < 1.653$	$72\phi \times 38\eta$		$36\phi \times 38\eta$
HCAL $1.653 < \lvert\eta\rvert < 2.001$	$72\phi \times 8\eta$		$36\phi \times 4\eta$
HCAL $2.001 < \lvert\eta\rvert < 2.262$	$72\phi \times 4\eta$		$36\phi \times 2\eta$
HCAL $2.262 < \lvert\eta\rvert < 2.61$	$72\phi \times 4\eta$		$36\phi \times 4\eta$

Table 2: CMS calorimeter and trigger tower granularity.

transverse energy in the corresponding region is required to be less than 1 GeV.

2.5 Jet Trigger Algorithm

The jet trigger algorithm based on the sliding window trigger tower granularity (see table 2) involves the sums of transverse energy in trigger towers within nonoverlapping regions of $0.35\phi \times 0.35\eta$, i.e. $4\phi \times 4\eta$ trigger tower sums. Sums of transverse energies in $0.7\phi \times 0.7\eta$ regions calculated using these $0.35\phi \times 0.35\eta$ sums with complete overlap and spanning the detector are also considered for the jet trigger. Missing E_t, single hadron and total E_t triggers also make use of the $0.35\phi \times 0.35\eta$ transverse energies.

3 Calorimeter and Trigger Tower Granularity

The CMS calorimeter and trigger tower granularity is shown in Table 2. Note that in the region of $1.566 < |\eta| < 1.653$, where the ECAL towers are missing, the energy from the first 25 X_0 of HCAL tower is used as an EM trigger tower to maintain good acceptance for the electron/photon trigger.

For the "sliding window" trigger configuration there is a 1:1 correspondence between HCAL and ECAL trigger towers. The trigger tower size is equivalent to the HCAL physical towers, $0.0873\phi \times 0.0873\eta$. The ϕ size remains constant in $\Delta\phi$ and the η size remains constant in $\Delta\eta$ down to an η of 2.1, beyond which the η size doubles.

For the "peak finding" trigger electron identification logic, the ECAL trigger cells are up to one third the size of the HCAL physical towers in η but are twice as coarse in their size in ϕ. The "peak finding" trigger configuration adapted for the $PbWO_4$ calorimeter approximates the original scheme proposed for the shashlik calorimeter in [4] as closely as possible.

The boundaries of HCAL trigger towers line up with boundaries of the ECAL trigger towers in η and ϕ for both the trigger schemes.

4 Level 1 Calorimeter Trigger Design

The level 1 calorimeter trigger system (See Figure 3) consists of regional and global processors. The regional system processes the electromagnetic and hadronic trigger tower sums from the calorimeter front end electronics and delivers regional information on electrons, photons, jets and partial energy sums to the global calorimeter level 1 trigger system. The regional system begins after the data from the front end electronics is received on optical fibers and translated to signals on copper and ends with cables that transmit the results to the calorimeter global level 1 trigger system.

After establishing requirements for the performance of the trigger system [5, 6] which fulfill the physics goals of the CMS experiment, we have produced a conceptual design [1] of the level 1 calorimeter regional trigger system based on the "sliding window" algorithm. The input data to the regional trigger processor consists of ECAL and HCAL transverse energies arranged in $72\phi \times 54\eta$ trigger towers of size $0.087\phi \times 0.087\eta$ each. Each regional processor crate contains up to 8 Receiver cards, 8 Electron Isolation cards, a Jet/Summary card, a Readout Controller card and other support cards. It is designed to fully process upto 256 trigger towers. One of the main challenges in achieving a compact configuration is the sharing of data between these cards. In this design we have limited the dynamic range of the data that is shared between the neighbors, with the realization that these data are used only for cutting on neighboring energies, and, therefore their dynamic range need to extend only up to realistic cut values. Simulation results presented below include details such as data transmission scales with limited dynamic range, resolution and integer arithmetic.

5 Simulation Program

5.1 Particle Tracking

We have used the Pythia Monte Carlo program to simulate several hundred thousand QCD jet and other events. The response of the CMS detector was simulated for these events using a simplified geometry (See Table 3 for detector geometrical parameters used) with a parameterized detector response. Particle tracking through the tracking volume in the magnetic field ($B_z = 4$T) is done using a helical path for charged particles and straight lines for neutral particles, ignoring dE/dx energy loss. Electron bremsstrahlung and photon conversions in the tracking material are simulated using a uniform medium within the tracking

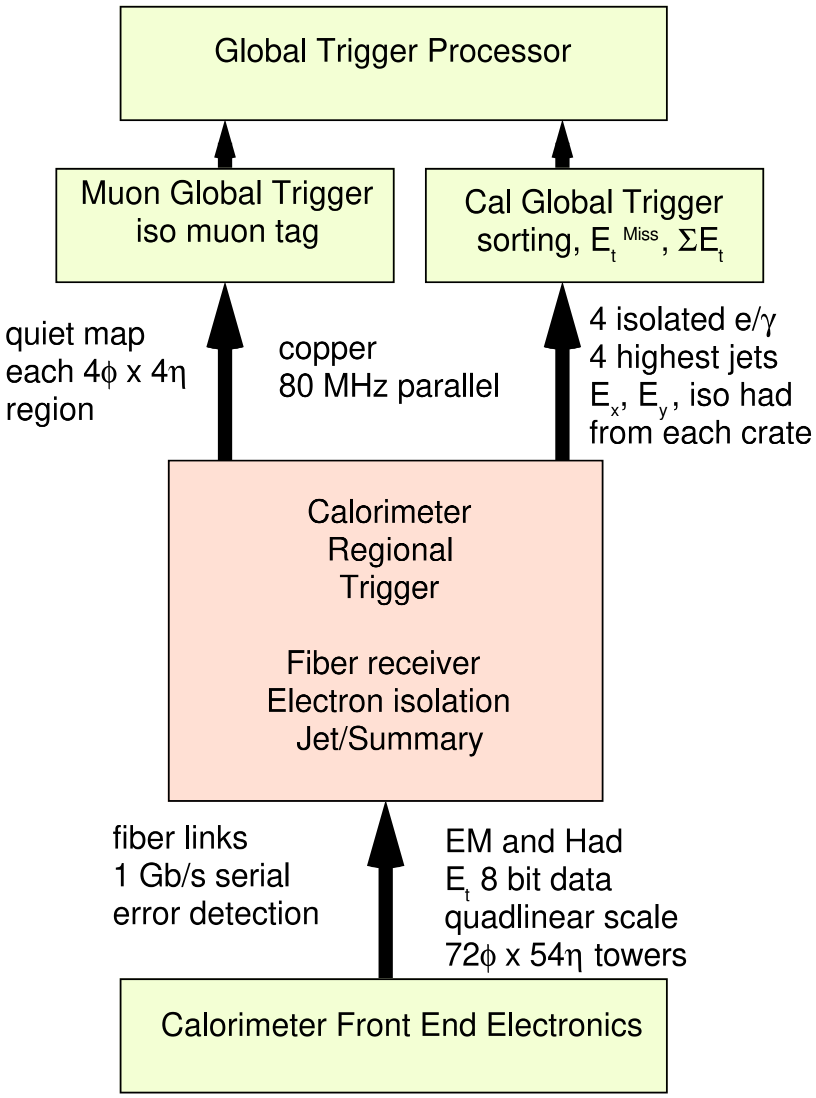

Figure 3: CMS level 1 calorimeter trigger overview.

Item	Value
Magnetic field in tracker	4.0 T
Tracking volume radius	1.5 m
Tracker thickness	0.2 X_0
Barrel preshower inner radius	1.37 m
Barrel preshower thickness	Pb 3.0 X_0
Barrel ECAL inner radius	1.43
ECAL tower tilt in degrees	3 °
ECAL barrel tower thickness	$PbWO_4$ 25. X_0
Endcap preshower Z_{min}	3.05
Endcap preshower thickness	Pb 3.0 X_0
ECAL endcap η_{min}	1.653
ECAL endcap Z_{min}	3.2 m
ECAL endcap tower thickness	$PbWO_4$ 25. X_0
HCAL barrel inner radius	1.86 m
HCAL barrel outer radius	2.864 m
HCAL endcap Z_{min}	3.78 m
HCAL endcap Z_{max}	5.6 m
HCAL material	Cu-Scin

Table 3: CMS detector geometrical parameters

volume equivalent to a thickness of 0.2 X_0. Meson decays within this tracking volume are also implemented. Particles are thus tracked up to the face of the preshower detector.

5.2 Shower Parameterization

After the particles are tracked the to face of the preshower detector, the parameterized response of electrons and photon showers is calculated. The energy of the electrons and photons is smeared with the expected detector resolution of $\Delta E = .03\sqrt{E} + .005E$. The shower development in the calorimeter is then calculated, ignoring magnetic field effects, i.e. the shower is developed along the direction of the initial particle at the face of the preshower detector. The longitudinal distribution of electron and photon showers is parametrized as a gamma distribution, as described by the Particle Data Group [7]. Shower parameters were obtained from full GEANT simulation (See Figure 4) of electron showers in the $PbWO_4$ crystals. The longitudinal distribution is fluctuated by a scale factor which is normally distributed, with the parameter set to most accurately duplicate the amount of energy electrons deposit beyond 25 X_0. The same parametrization is used in the preshower detector, scaled by radiation lengths to account for the different material. Similarly, a GEANT simulation was used to determine the behavior of electron showers in the hadronic section. The energy loss along the shower is subtracted in 2 mm steps through the preshower detector and 1

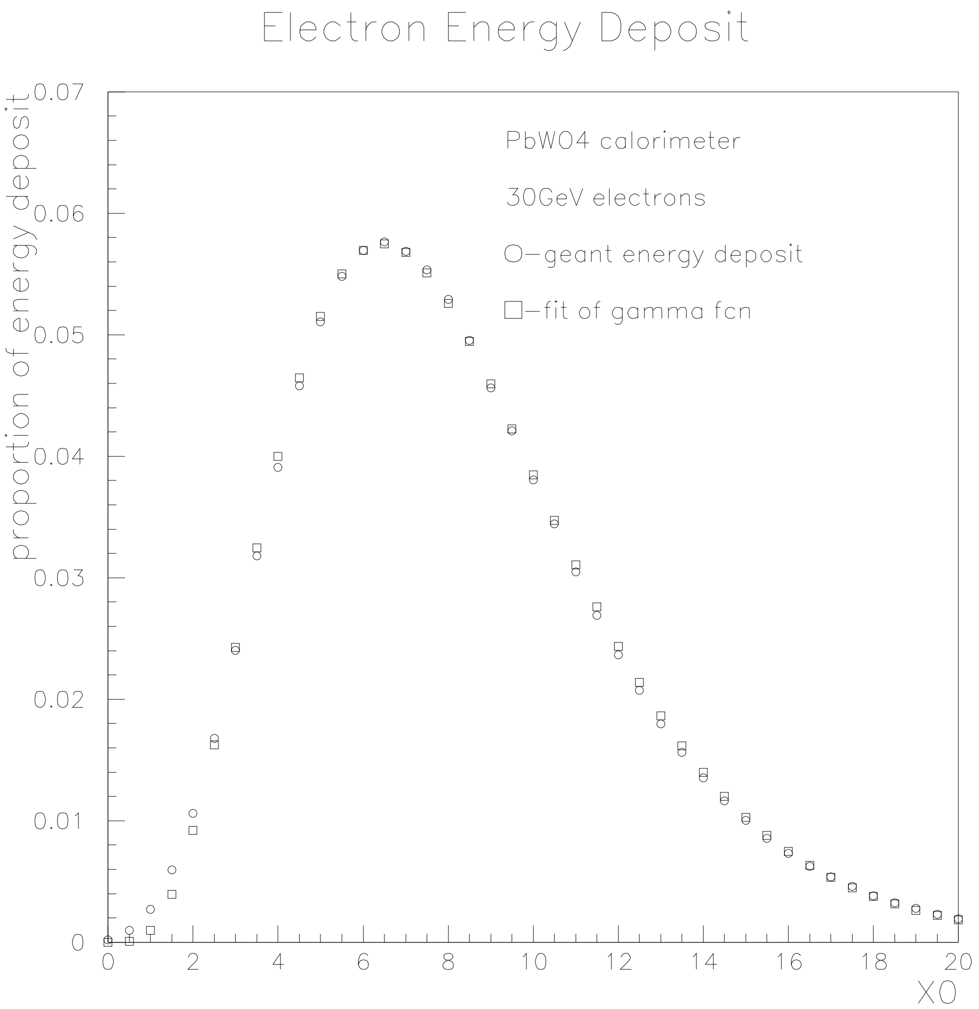

Figure 4: Energy loss versus depth of the shower in units of radiation length in the $PbWO_4$ from GEANT simulation. The fit parameters are used to provide fast shower simulation.

cm steps in the electromagnetic calorimeter, until all the particle energy is deposited. At each step, three deposits of energy are distributed transversely such that 90% of them are contained within 1 Moliere radius and 99% are contained within 3 Moliere radii using a double gaussian distribution. These subdivided deposits of energy at each step are stored as calorimeter hits.

Muons are tracked through the preshower and calorimeter along the direction of the particle at the face of the calorimeter depositing dE/dx energy along their tracks. The dE/dx energy deposits are also stored as calorimeter hits.

All other charged particles, i.e. pions and kaons, are tracked similarly to the muons until they interact according to the hadronic interaction probability. The energy of the hadrons is then smeared with the expected detector resolution of $\Delta E = .8\sqrt{E} + .03E$. A parameterization [8], with separate gamma distribution shape for electromagnetic and hadronic components of the hadron shower, is used to calculate the energy deposits of the hadrons in 30 cm steps (in the HCAL) along the direction of the shower. Although more accurate parameters can be obtained by fully simulating a large number of hadron showers using a program such as GEANT/GHIESHA, we chose to use the parameters given in [8]. Because this parameterization is in terms of the properties of the medium such as radiation and interaction lengths, we believe that it scales suitably to the CMS Cu-Scintillator calorimeter. To simulate the transverse development of the shower, at each 30 cm step three deposits of energy are distributed transversely with a double exponential distribution [9]. The parameters in that distribution are scaled to reflect the difference in interaction lengths in the different media. These subdivided deposits of energy at each step are stored as calorimeter hits.

5.3 Simulation of Calorimeter Data

The calorimeter hits are summed to provide the total energy in each calorimeter tower. Gaussian noise is then added at the level of .15 GeV for ECAL and HCAL towers. Cutoffs (ECAL cutoff = .3 GeV and HCAL cutoff = .3 GeV) on the energy thus simulated are applied to suppress noise before transverse energies are computed using tower center coordinates. The appropriate number of calorimeter tower energies (See Table 2) are added to obtain the sliding window and peak finding trigger tower energies.

Both ECAL and HCAL trigger tower data were further reduced in resolution and dynamic range to account for the 8 bit quadlinear scale (See Table 1) transmission from the front end electronics to the trigger through the fiber optic system. For the sliding window electron/photon algorithm, the ECAL and HCAL energies are provided on an 8-bit linear scale with 0.5 GeV resolution. In order to reduce the number of bits of information exchanged between electronics cards, the dynamic range of neighboring tower HCAL information is limited to 2 bits. Overflows of both the 8 bit scale for ECAL and central HCAL towers, and 2 bit scale for neighboring HCAL towers are treated as maxima. For the peak finding algorithm the trigger tower data are provided on an 8-bit linear scale with 1 GeV resolution.

5.4 Occupancy

100000 minimum bias events, including elastic, diffractive and low-p_t jet production, were simulated using Pythia and stored in a database. The cross section for this set of events is 156 mb which results in 39 events per interaction for the full LHC luminosity of $10^{34}\text{cm}^{-2}\text{s}^{-1}$. Multiple interactions per crossing were simulated by adding data from this database based on a poisson distributed random selection of events corresponding to the luminosity for the run. Unless otherwise stated, all data for rates and efficiency presented in this paper are for a luminosity of $10^{34}\text{cm}^{-2}\text{s}^{-1}$.

The occupancy for QCD 2-jet background and minimum bias events is shown for ECAL and HCAL towers in Figures 5 and 6. The lowest lying points are for minimum bias events. The data for jet events has progressively higher occupancy as the p_t range for the jet events is increased. These plots show that the calorimeter tower energy cutoffs of 0.3 GeV remove most of the uniformly distributed background energy. However, the large addition of minimum bias events due to multiple interactions could and does yield occasional events with overlapping towers with minimum bias energy over these thresholds. A more serious problem is expected in the endcap region where leakage energy from the proton remnants is expected. When these types of energy deposits occur within the isolation region of the electron/photon trigger we expect inefficiencies. However, it is shown in the data below that a suitable choice of cutoffs has essentially eliminated any inefficiency due to these problems.

6 Electron/Photon Trigger Rates and Efficiency

6.1 Sliding Window Algorithm

We have simulated the sliding window algorithm, including the details of bit resolution and dynamic range as designed in the hardware, and obtained the electron/photon trigger QCD background rate and efficiency for detecting single electrons with minimum bias background. The integrated rates[2] from QCD two jet production background including minimum bias overlay are shown after the various cuts used for the sliding window algorithm in Figure 7. The efficiency for triggering on isolated single electrons with the inclusion of minimum bias overlays is shown in Figure 8. It is seen that hadronic isolation provides most of the rate reduction with high efficiency. The rate of 24 kHz for an E_t cutoff of 30 GeV and no other cuts for a single electron/photon trigger is reduced to 11 kHz after the H/E cut and further down to 5.7 kHz after the transverse HAD isolation cut. The EM isolation cut value is adjusted so that the efficiency is held high. In spite of this fairly tight EM cut the additional rate reduction due to EM isolation, i.e. from 5.7 kHz to 4.7 kHz, is only marginal.

The electron trigger efficiency plot (see Figure 8) shows that an E_t cutoff of 30 GeV provides full, i.e. $> 95\%$, efficiency above a p_t of 40 GeV. Our earlier studies [6, 5], which did not include the preshower detector because they simulated the CeF_3 calorimeter, showed better efficiency turn-on curves. The energy deposited in the preshower detector cannot be

[2] The integrated rate of triggers above a cutoff is plotted versus cutoff transverse energy

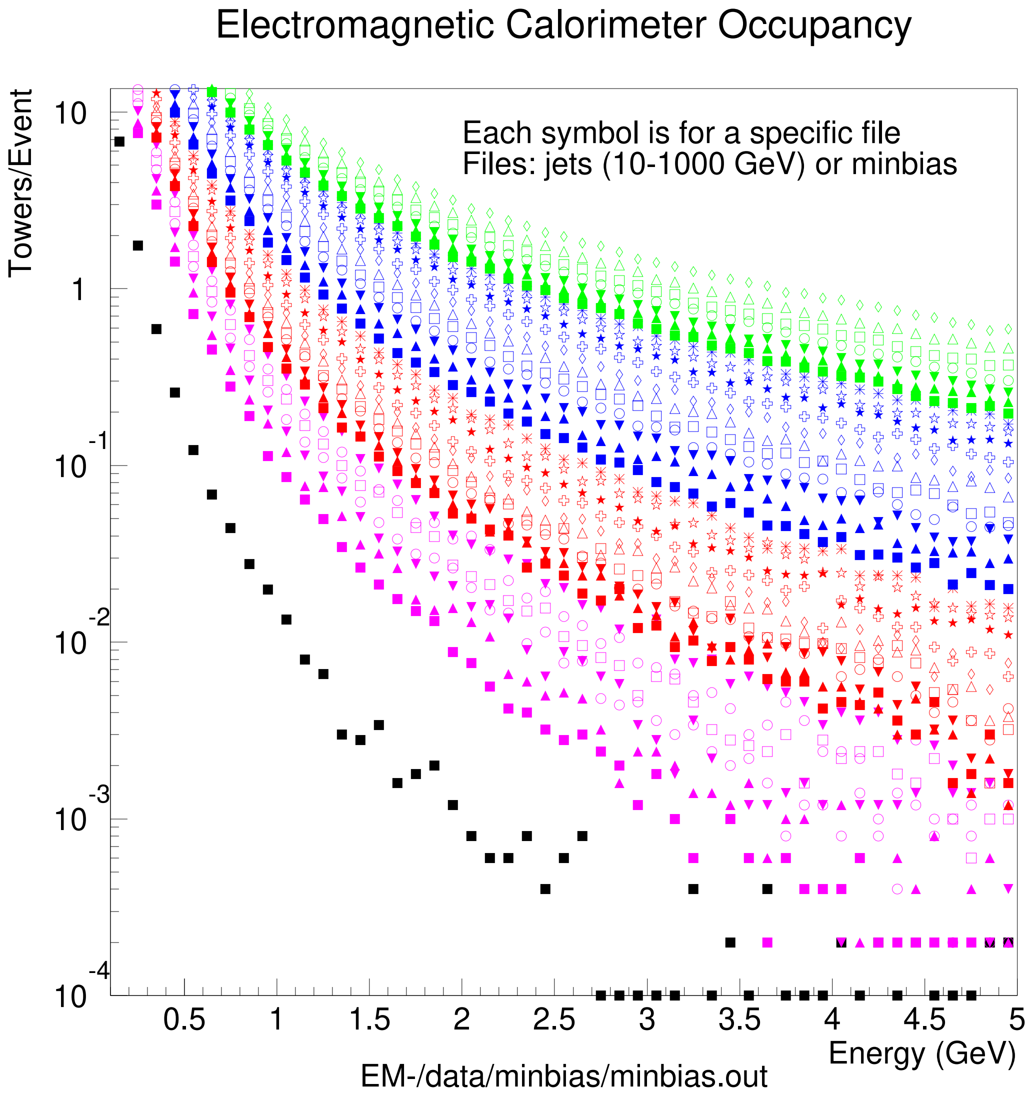

Figure 5: Occupancy, i.e. towers per event with energy above energy cutoff, is plotted versus energy cutoff for ECAL towers for different p_t ranges of QCD 2-jet and minimum bias event data. The symbols shown on the plot from lowest to highest correspond to minimum bias, then jet p_t ranges (in GeV) 10-12, 12-14, 14-16, 16-18, 18-20, 20-22, 22-24, 24-26, 26-28, 28-30, 30-32, 32-34, 34-37, 37-40, 40-45, 45-50, 50-55, 55-60, 60-70, 70-80, 80-90, 90-100, 100-115, 115-130, 130-150, 150-175, 175-200, 200-225, 225-250, 250-275, 275-300, 300-350, 350-400, 400-500, 500-700, and 700-1000.

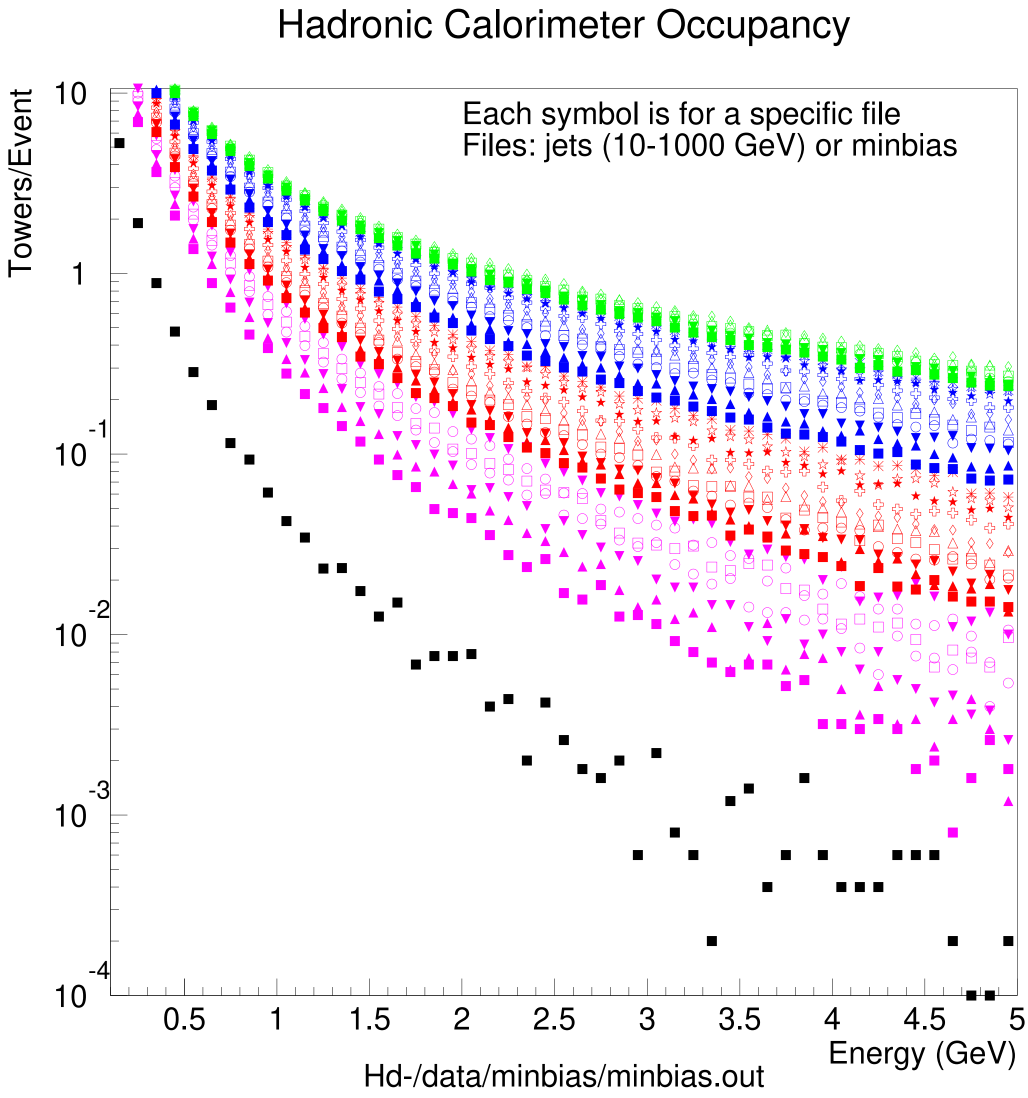

Figure 6: Occupancy, i.e. towers per event with energy above energy cutoff, is plotted versus energy cutoff for HCAL towers for different p_t ranges of QCD 2-jet and minimum bias event data. The symbols shown on the plot from lowest to highest correspond to minimum bias, then jet p_t ranges (in GeV) 10-12, 12-14, 14-16, 16-18, 18-20, 20-22, 22-24, 24-26, 26-28, 28-30, 30-32, 32-34, 34-37, 37-40, 40-45, 45-50, 50-55, 55-60, 60-70, 70-80, 80-90, 90-100, 100-115, 115-130, 130-150, 150-175, 175-200, 200-225, 225-250, 250-275, 275-300, 300-350, 350-400, 400-500, 500-700, and 700-1000.

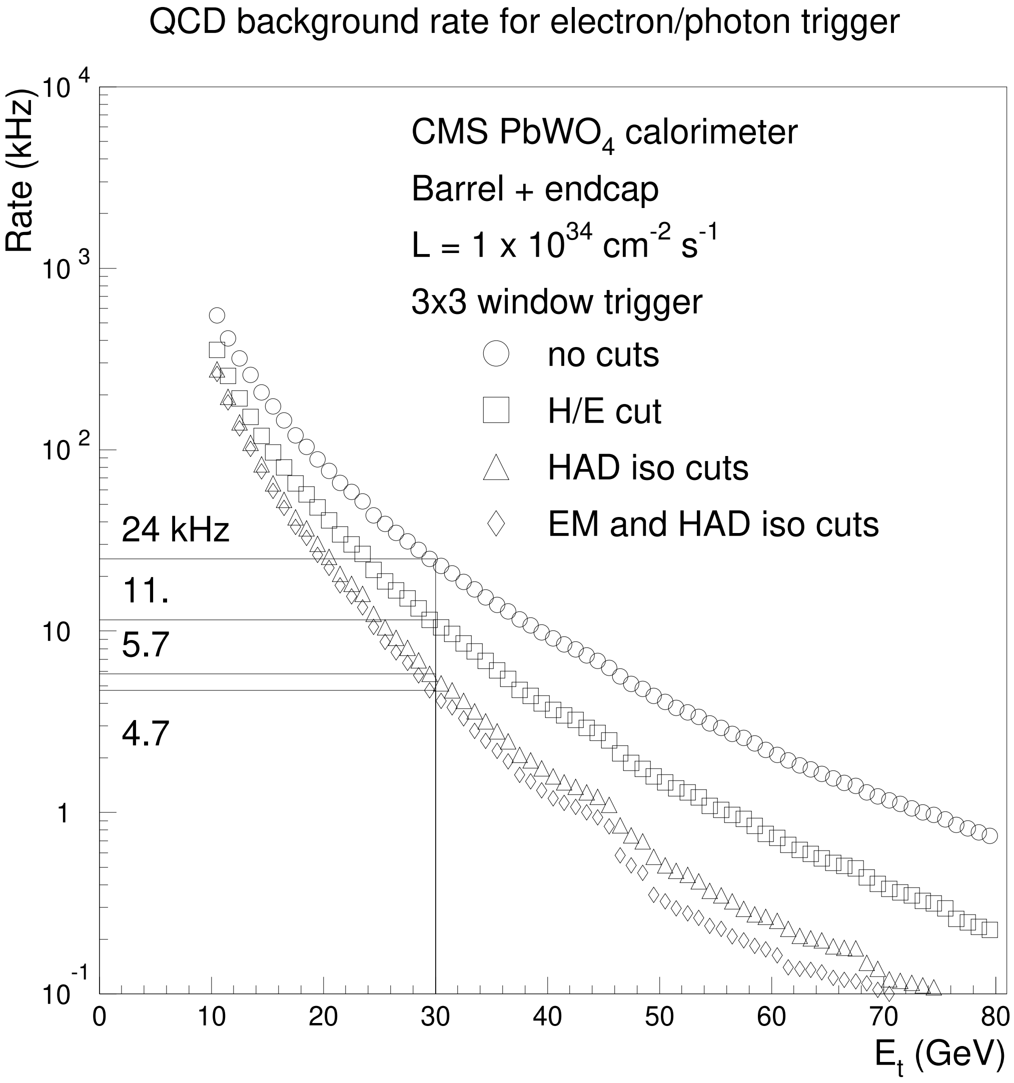

Figure 7: Sliding window single electron/photon trigger QCD background integrated rate, including minimum bias for nominal luminosity, for various cuts.

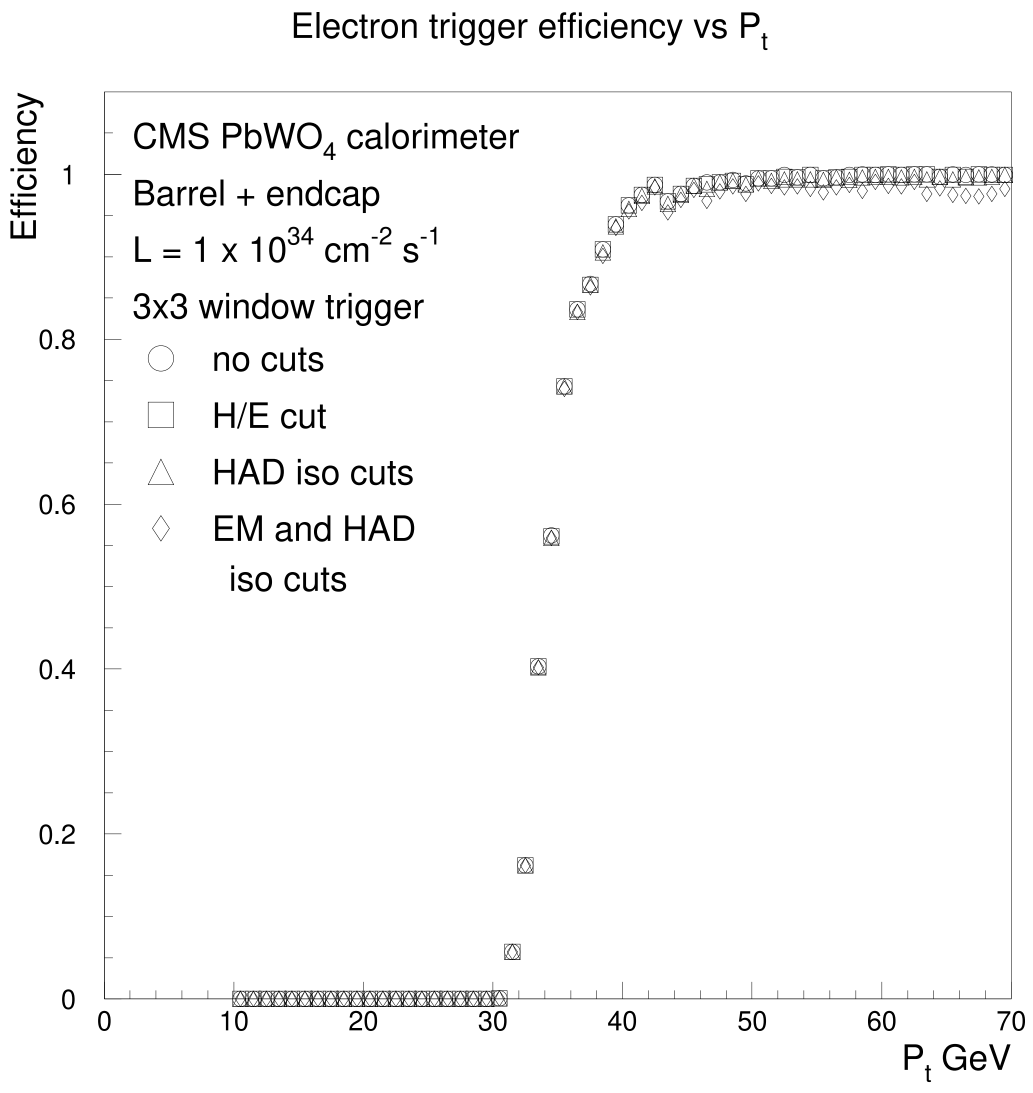

Figure 8: Sliding window electron/photon trigger efficiency for triggering on single electrons, including minimum bias for nominal luminosity, for various cuts.

included in the calorimeter trigger. Therefore, in this study the energy deposited in 3 X_0 preshower detector is not included in the trigger tower energies and it acts as an additional cutoff on the EM energy deposits.

6.2 Performance of EM Isolation

Figure 9 shows that the efficiency of the electron/photon trigger is high ($> 95\%$) over the full η range, for all cuts, except for the tightest EM isolation cut of 1 GeV. The transverse isolation cuts have been disabled in the region of the ECAL tower gap where the energy from the first 25 X_0 of HCAL tower is used as EM energy. As seen in the rate plot, Figure 7, the nominal EM isolation cut of 2 GeV does not yield a significant reduction in the background rate. This cannot be improved since further tightening of this cut yields poor efficiency, particularly in the $\eta \approx 0$ and endcap regions. The loss of efficiency in the region close to $\eta = 0$ is due to the interplay of the calorimeter energy cutoffs set in total energy scale to suppress noise and the loss of energy in the preshower detector. At moderate values of $|\eta|$ the calorimeter total energy cutoffs and the energy loss in the preshower (which is always 3 X_0) are small enough that they do not effect the electron trigger algorithm which is performed on a transverse energy scale. At large $|\eta|$ in the endcap ECAL, the physical tower sizes are small and the leakage energy is important. Often there is energy leakage into several calorimeter towers that results in an EM isolation inefficiency. This effect persists in spite of attempts to reduce it by doubling the η-range of the trigger tower to calorimeter tower mapping at high $|\eta|$ (see Table 2).

6.3 Single inclusive electrons from W and top events

An important test of the electron trigger involves simulation of events with electrons from real physics sources combined with the QCD 2-jet and minbias overlay background. Such events have more activity than combinations of isolated electrons with the QCD 2-jet and minbias overlay background. The sliding window trigger efficiencies for electrons from Drell-Yan W and top decay events, including the minimum bias event overlay for the case of $10^{34}\mathrm{cm}^{-2}\mathrm{s}{-1}$ luminosity, are plotted in Figures 10 and 11. These data show that the efficiency for finding isolated electrons by the sliding window algorithm in W and top events is also quite high. Although the statistics are low for these data, some small additional loss in efficiency is seen for these events, particularly for electrons from top decay events. The efficiency for W and top decay electrons exceeds 95% and 90% for $p_t > 40$ GeV, respectively. The loss in efficiency for top decay electrons is expected due to the proximity of jets to some of these electrons. This loss is reduced by only using HAD isolation and not using EM isolation. In addition, the HAD isolation can be removed above a threshold of about 50 GeV, assuring high efficiency for the highest p_t events.

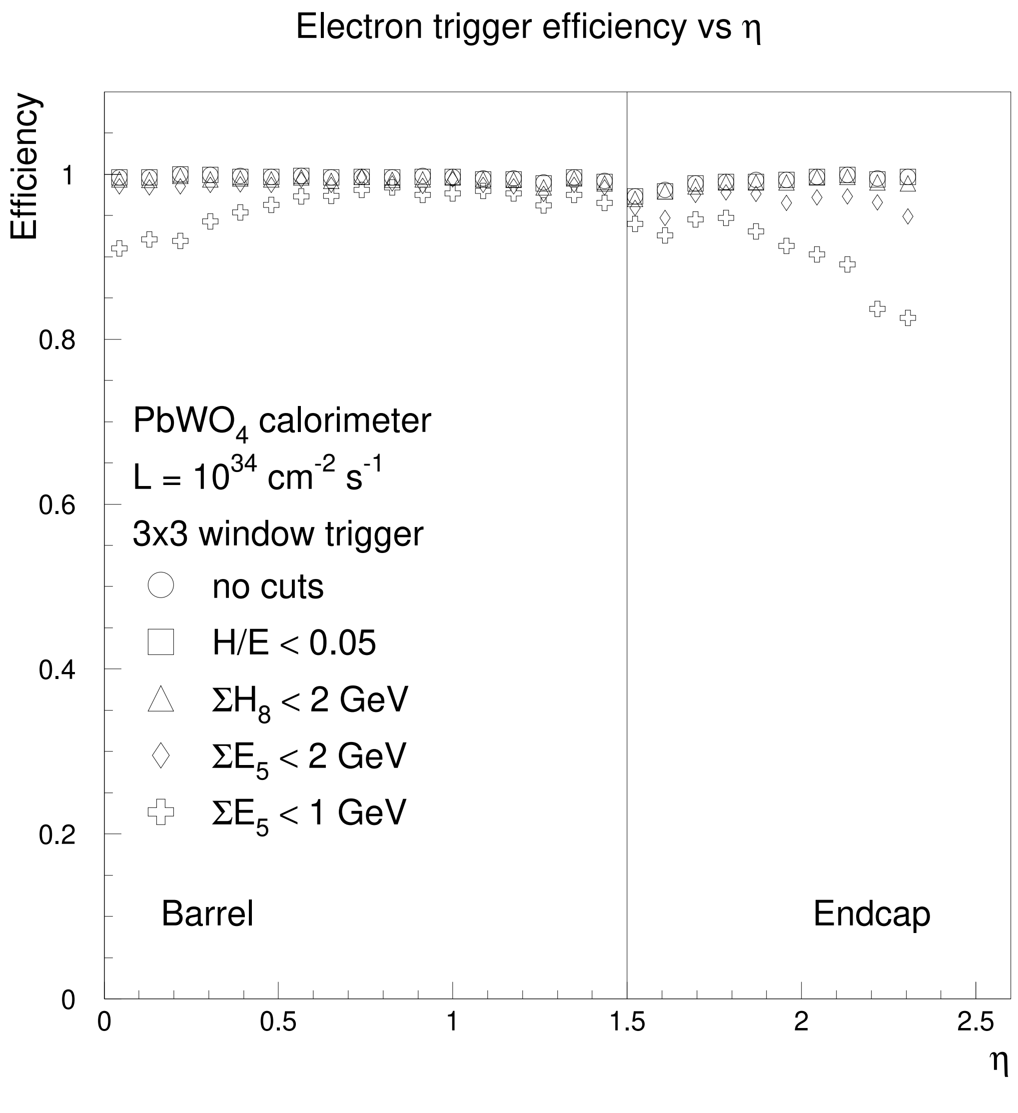

Figure 9: Sliding window trigger efficiency for finding single isolated electrons with the inclusion of minimum bias events at full luminosity plotted versus η.

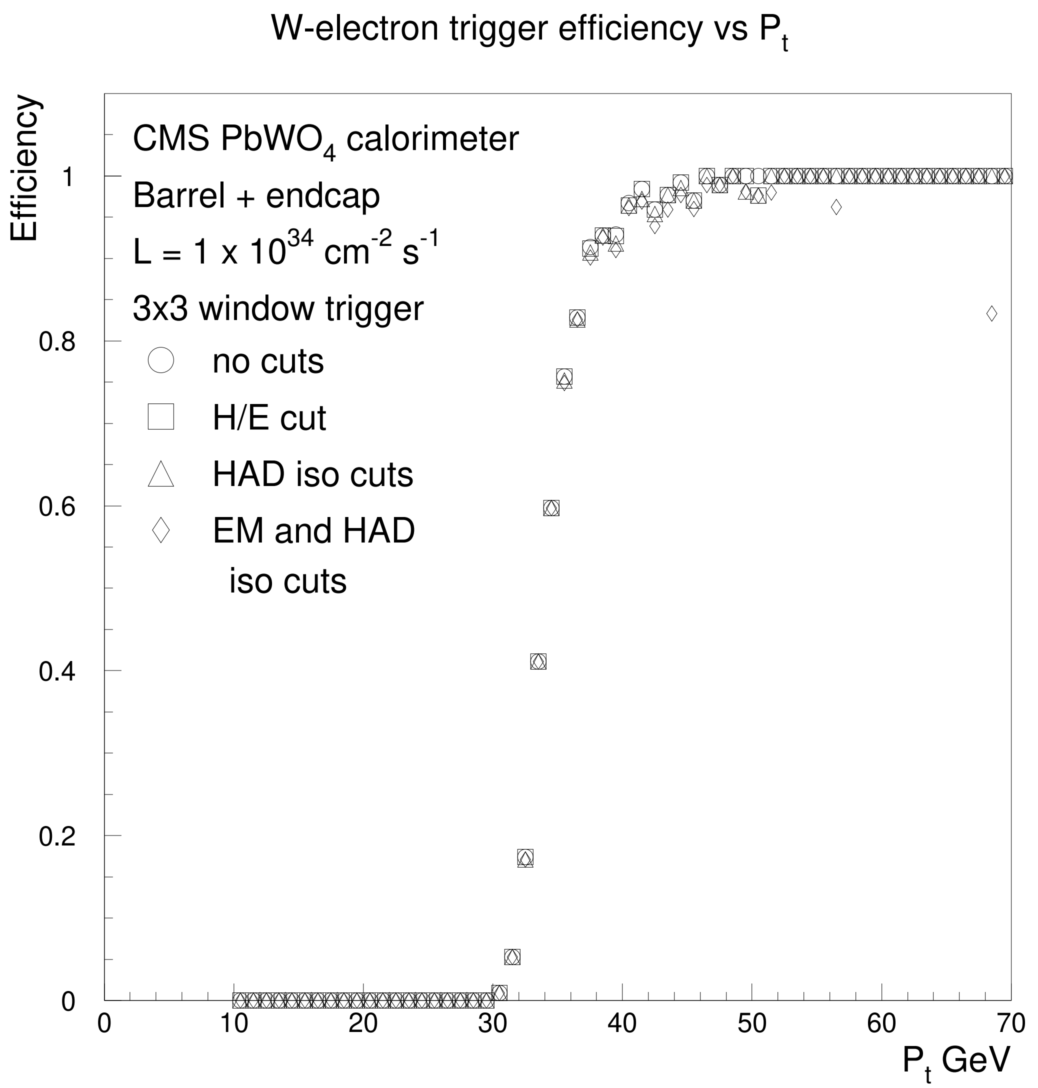

Figure 10: Sliding window trigger efficiency for finding electrons from Drell-Yan W events.

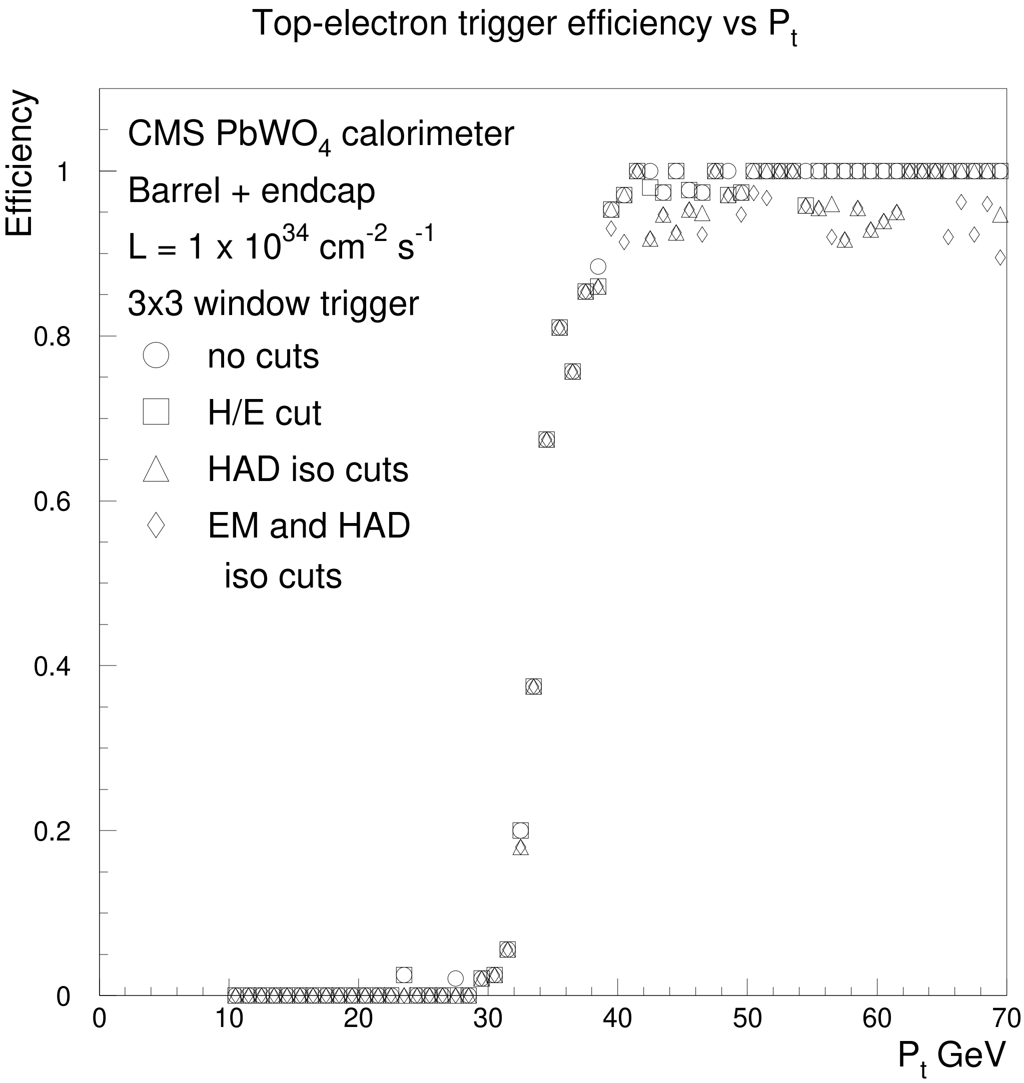

Figure 11: Sliding window trigger efficiency for finding electrons from top decay events.

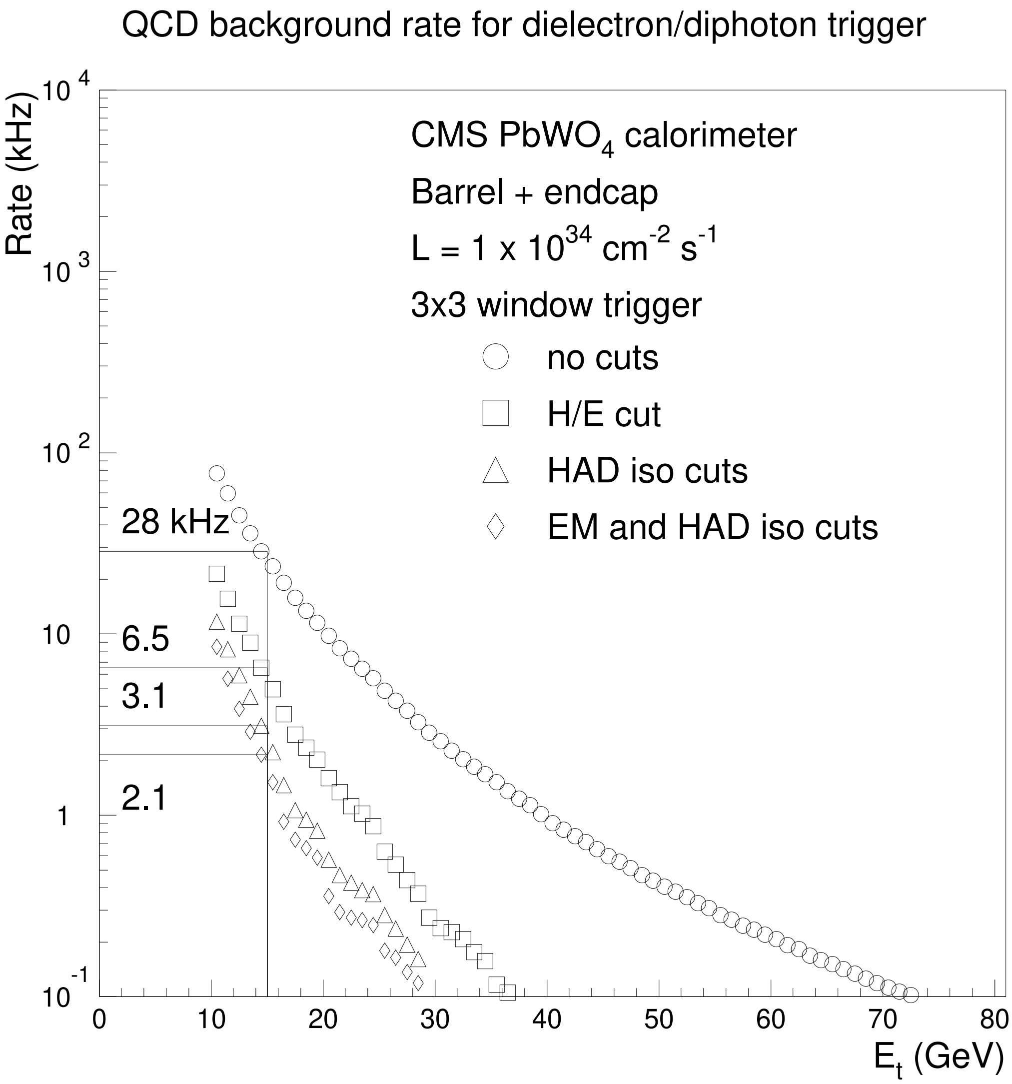

Figure 12: 3x3 sliding window algorithm QCD background rate for diphoton/dielectron trigger for various isolation cuts.

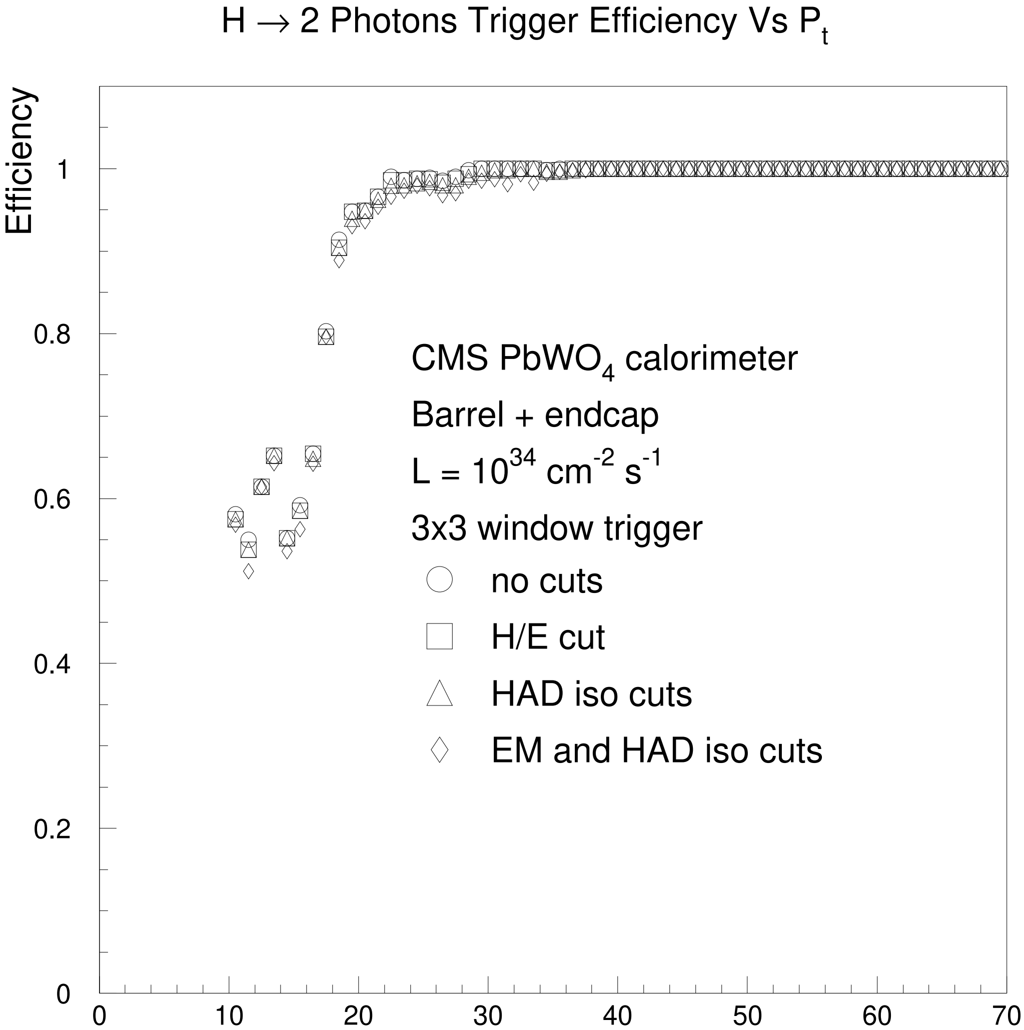

Figure 13: 3x3 sliding window algorithm QCD background rate for diphoton/dielectron trigger and efficiency for triggering on two photons from Higgs ($M_H = 80$ GeV) decay.

6.4 Dielectron/Diphoton Trigger

The dielectron/diphoton QCD background rate and efficiency for detecting two photons from Higgs decay using the sliding window algorithm are shown in Figures 12 and 13. The integrated rate is plotted versus the trigger E_t cutoff required for both ECAL clusters. The efficiency is plotted versus the p_t of the lower energy photon. The of 28 kHz for an E_t cutoff of 15 GeV and no other cuts for the diphoton trigger is reduced to 6.5 kHz with H/E cut alone, and is further reduced to 3.1 kHz upon applying the transverse HAD isolation. EM isolation provides only a marginal additional reduction down to 2.1 kHz. The efficiency plot shows that, with an E_t cutoff setting of 15 GeV, the fully efficient p_t threshold is at 20 GeV. It is seen that the sliding window trigger satisfies the physics requirements of a few kHz rate and full efficiency above 20 GeV p_t for Higgs decays to two photons, with the use of transverse HAD isolation and without the use of EM isolation.

6.5 Sliding window trigger vs. changing luminosity

We have also studied the performance of the electron/photon trigger versus changing luminosity. At lower luminosity, we can employ a lower p_t cut trigger that does not require transverse isolation in order to have good efficiency for electrons from b decays. As an example, Figure 14 shows that an inclusive single electron trigger using the sliding window algorithm with only a threshold and H/E cuts yields rates of 3 kHz for E_t cutoffs of 11 and 28 GeV at luminosities of 10^{32} and 10^{33} cm^{-2}s^{-1}, respectively, while requiring transverse isolation yields a rate of 3 kHz for an E_t cutoff of 20 GeV at 10^{33} cm^{-2}s^{-1}. We see that at 10^{32} lower thresholds can be set for non-isolated electrons, using the H/E cut alone to obtain good efficiency for B physics. We also see that at 10^{33}, lower thresholds can be set using HAD isolation and due to the small isolation region ($.26\eta \times .26\phi$), good top efficiency can be attained. The use of tunable cut values, programmable energy scales, and separate and optional H/E and HAD transverse isolation cuts provide a powerful combination of parameters with which to optimize the trigger configuration for each luminosity setting.

6.6 Peak finding single electron trigger

We have simulated the peak finding algorithm, including the details of cluster codes and overlap detection as described in [3], and obtained the electron/photon trigger QCD background rate and efficiency for detecting single electrons with minimum bias background. The rates from the QCD two jet production background and the efficiency for isolated single electrons, including the minimum bias overlay, are shown with and without the HAD and EM isolation cuts of the peak finding algorithm in Figures 15 and 16. The rate of 26 kHz for an E_t cutoff of 30 GeV and no other cuts for the single electron/photon trigger is reduced to 5.6 kHz after the transverse HAD isolation cut alone. This result is in full agreement with the 5.7 kHz rate obtained for HAD isolation using the sliding window algorithm. As was the case for the sliding window algorithm, the additional reduction obtained by using EM transverse isolation (5.7 kHz reduces to 4.5 kHz) is marginal.

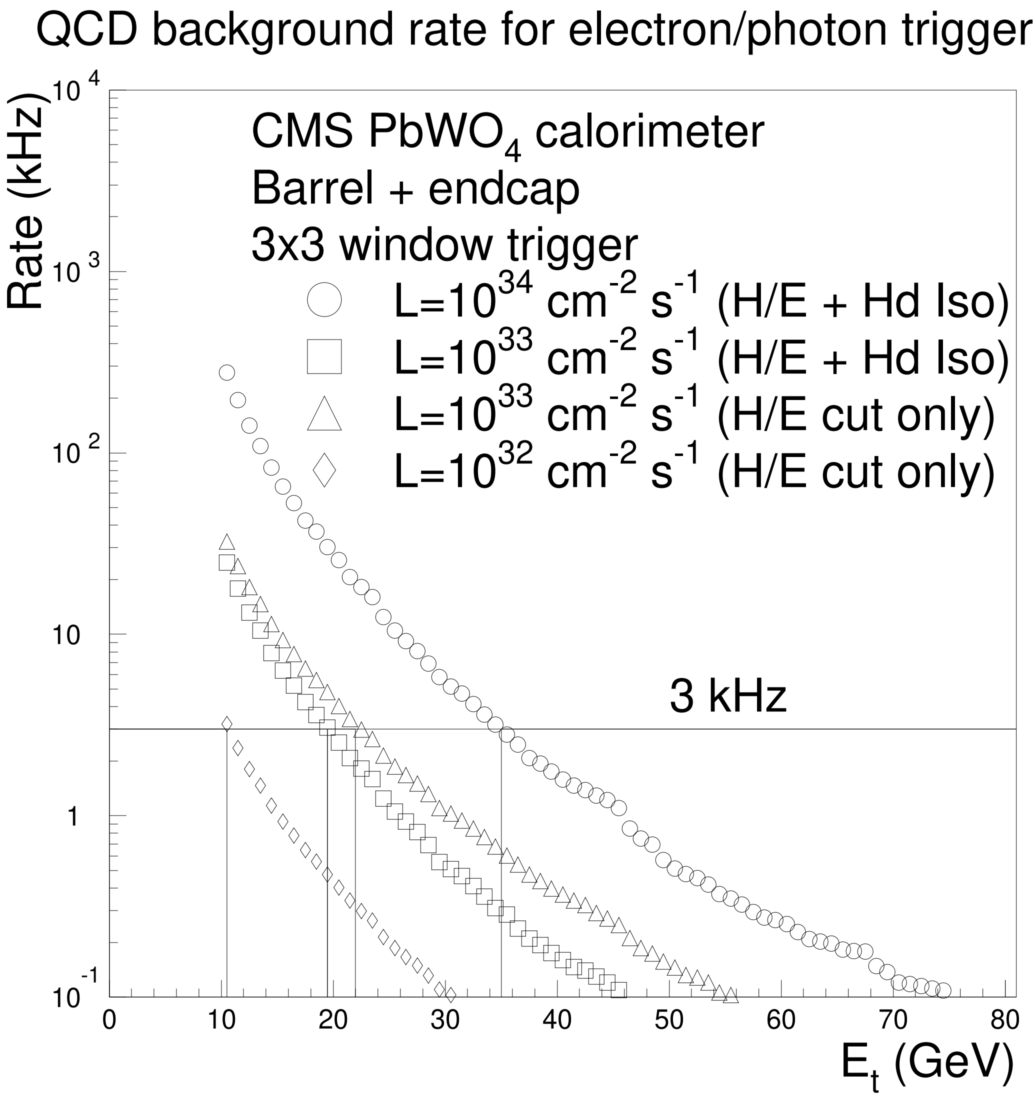

Figure 14: Sliding window algorithm QCD background rate for electron/photon trigger for luminosities of $10^{32-34}\mathrm{cm}^{-2}\mathrm{s}^{-1}$ with and without transverse hadronic isolation.

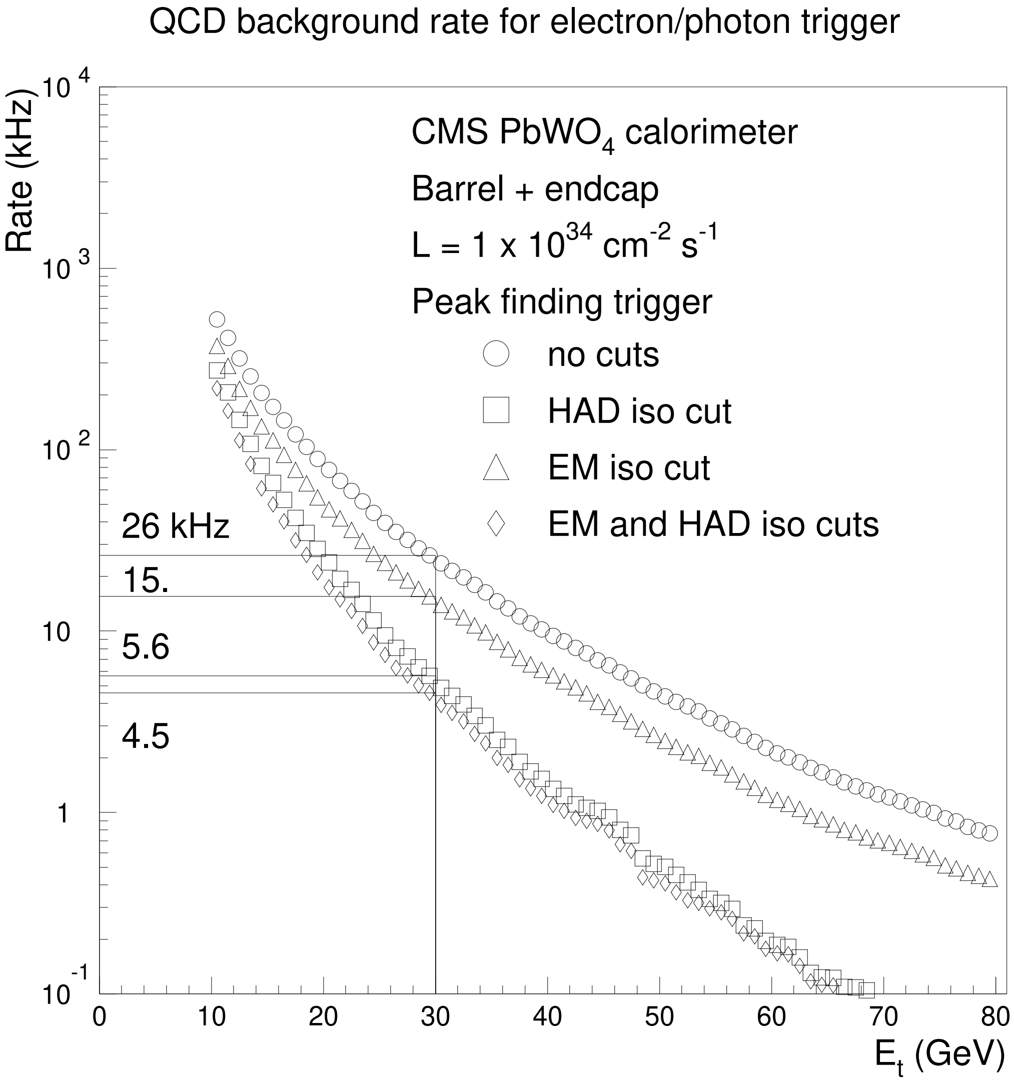

Figure 15: Peak finding single electron/photon trigger QCD background rate, including minimum bias for nominal luminosity, for various cuts.

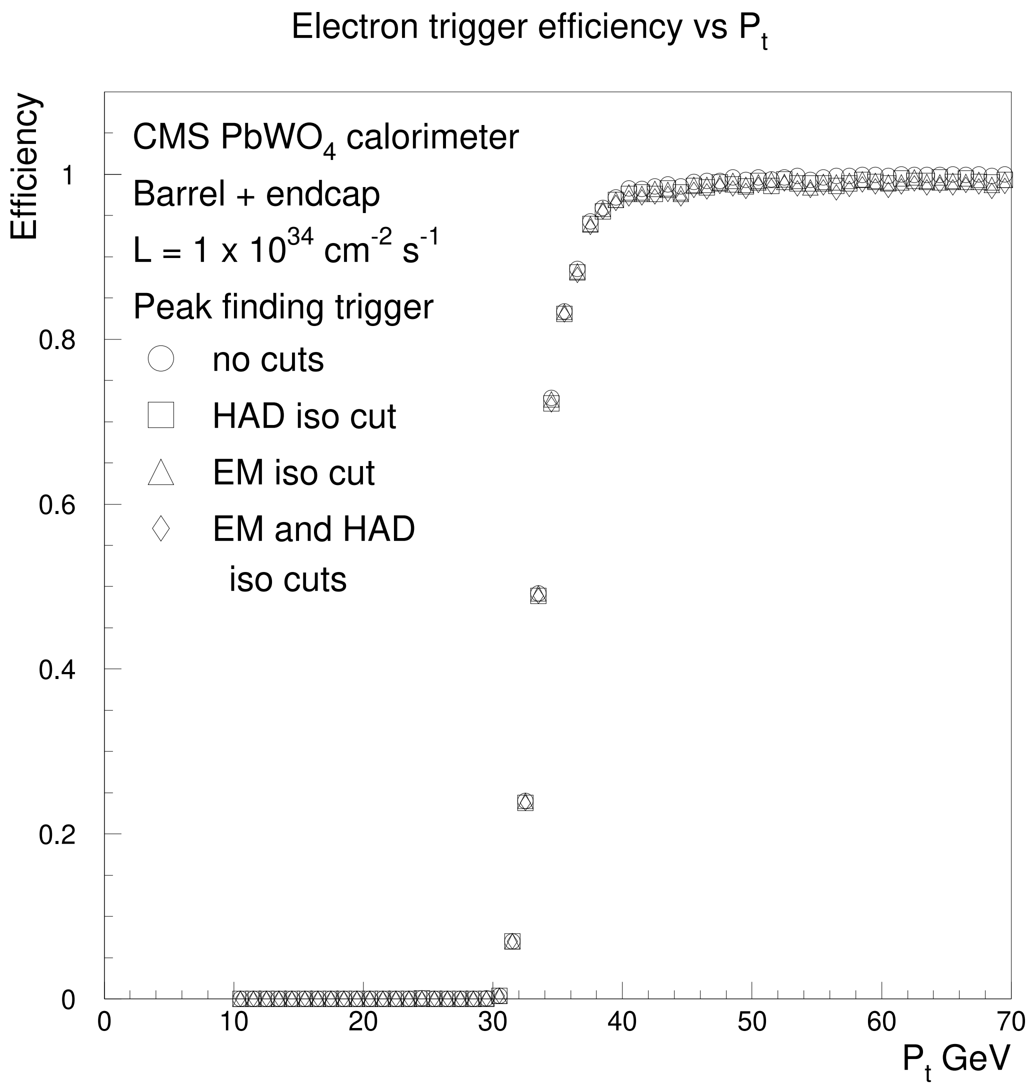

Figure 16: Peak finding single electron/photon trigger efficiency for triggering on isolated single electrons, including minimum bias for nominal luminosity, for various cuts.

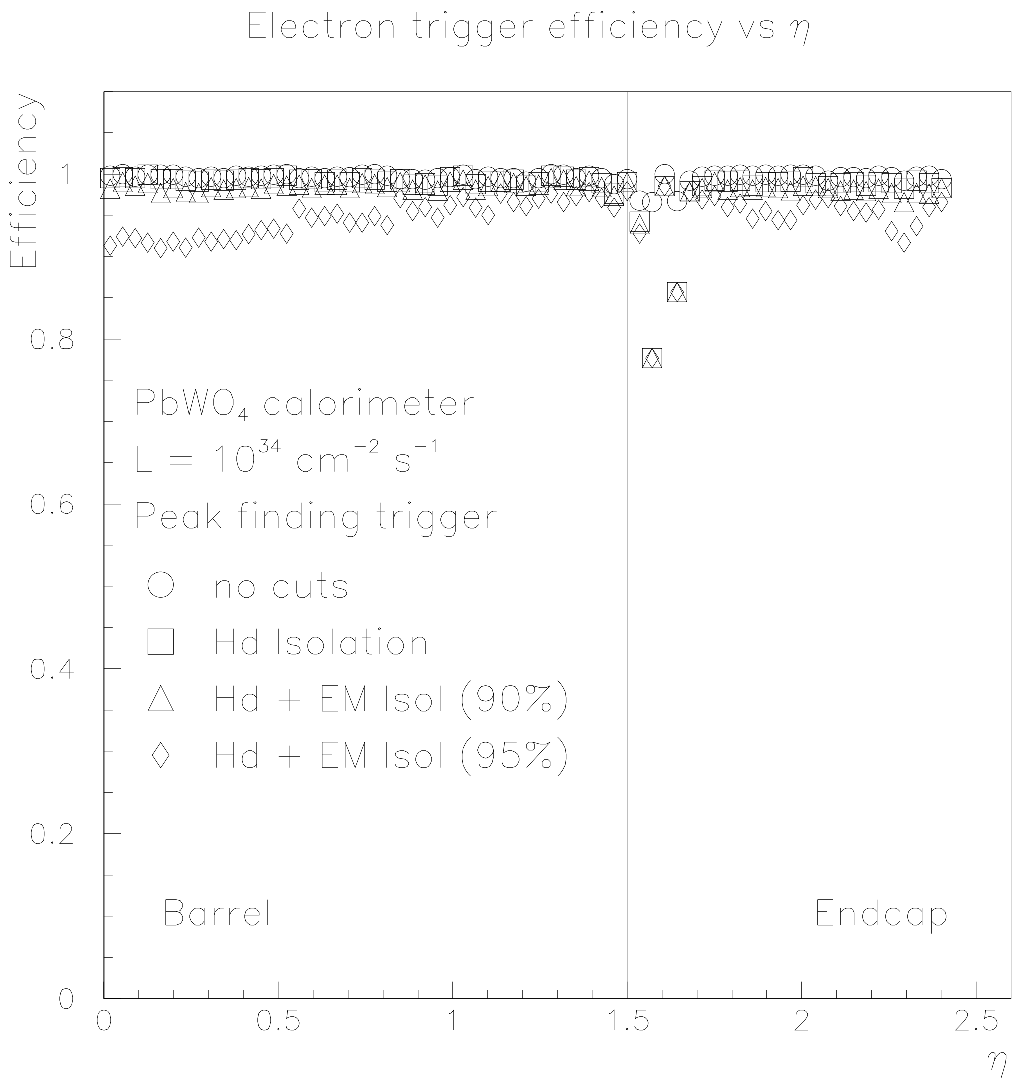

Figure 17: Peak finding trigger efficiency versus η for finding single isolated electrons with the inclusion of minimum bias events at full luminosity.

Figure 17 shows that the efficiency of the peak finding electron/photon trigger is high ($> 95\%$) over the full η range for the HAD isolation cut alone and somewhat lower for the nominal EM isolation cut(90%). There is some further loss of efficiency in the region of the ECAL tower gap ($|\eta|$ = 1.6 - 1.7) where the energy from the first 25 X_0 of HCAL tower is used as the EM energy. This is after attempts to remove the effect of the ECAL tower gap by disabling the transverse isolation in this region. As is seen in the rate plot, Figure 15, the nominal EM isolation cut of 90% in the peak finding algorithm does not yield significant reduction in the background rate. This cannot be improved because further tightening of this cut up to 95% yields poor efficiency, particularly in the $\eta \approx 0$ and endcap regions. The loss of efficiency for the peak finding trigger is due to the same reasons as discussed above for the sliding window trigger when its EM isolation cut was tightened. The leakage of EM energy into neighboring trigger towers in the forward regions persists in spite of the effort taken to reduce it by doubling the η-range of the trigger tower to calorimeter tower mapping at high $|\eta|$ (see Table 2).

6.7 Peak finding dielectron/diphoton trigger

The dielectron/diphoton QCD background rate and the efficiency for detecting two photons from Higgs decays using the peak finding algorithm are shown in Figures 18 and 19. The integrated rate is plotted versus the trigger E_t cutoff required for both ECAL clusters. The efficiency is plotted versus the p_t of the lower energy photon. The rate of 35 kHz for a 15 GeV E_t cutoff with no other cuts is reduced to 5.7 kHz using the HAD isolation cut alone. While the EM isolation does provide some additional rate reduction (5.7 kHz reduces to 2.3 kHz upon the requirement of EM isolation) with a small loss in efficiency, the total rates are already sufficiently low without the use of EM isolation.

6.8 Summary of electron trigger performance

The integrated rate and efficiency data presented above is summarized in Table 4. These data show that both the sliding window and peak finding algorithms perform identically for single and di- photon/electron triggers within the accuracy of these simulation results. The minor differences seen in Table 4 between the two algorithms are smaller than the variations caused by changing the cutoffs and isolation cuts. The differences are also smaller than the uncertainties inherent in the entire simulation procedure described here ranging from the use of shower parameterizations to the details of the detector design that are still being determined to the knowledge of the cross sections and physics details. What is important to note is that even considering these uncertainties, both the sliding window and peak finding single and di- electron/photon triggers clearly satisfy the CMS physics requirements at the full LHC design luminosity.

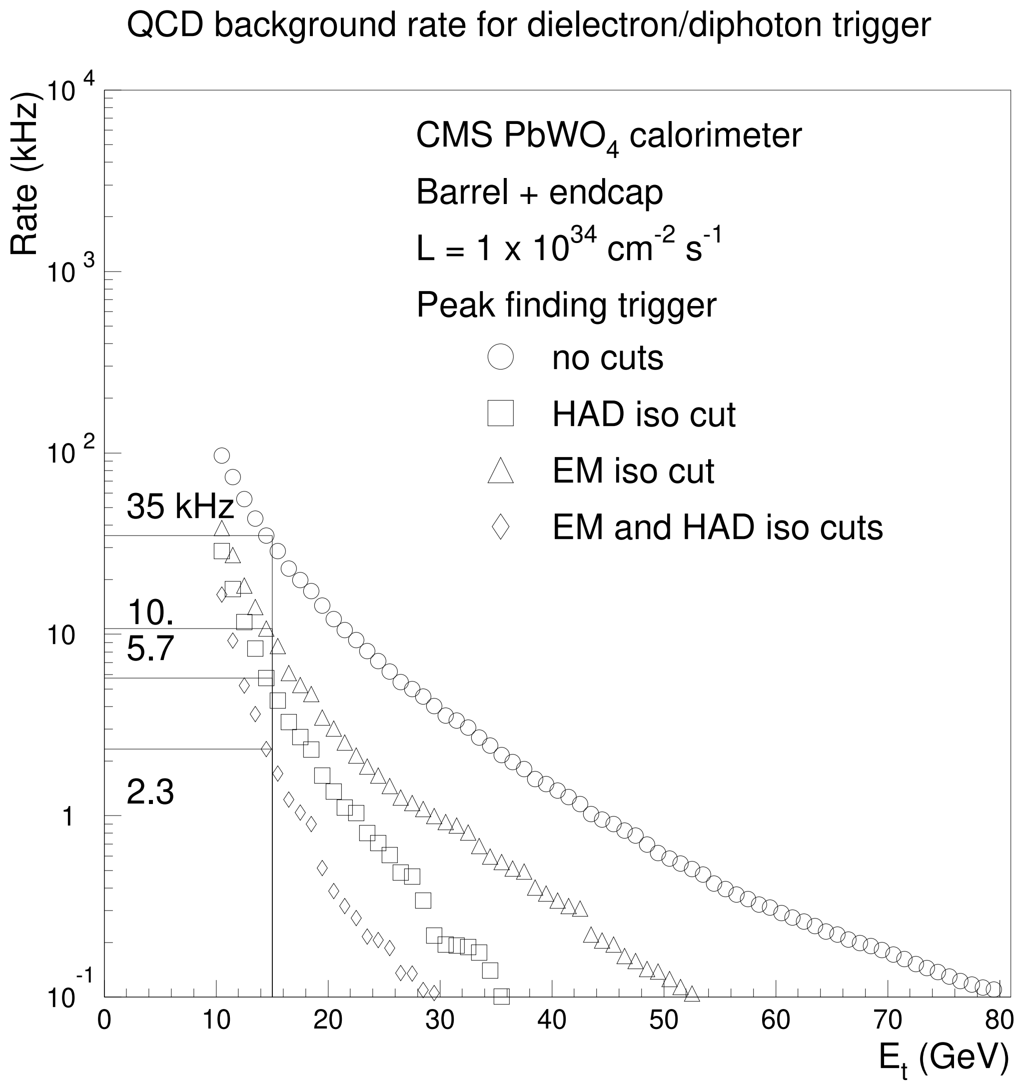

Figure 18: Peak finding algorithm QCD background rate for diphoton/dielectron trigger for various cuts.

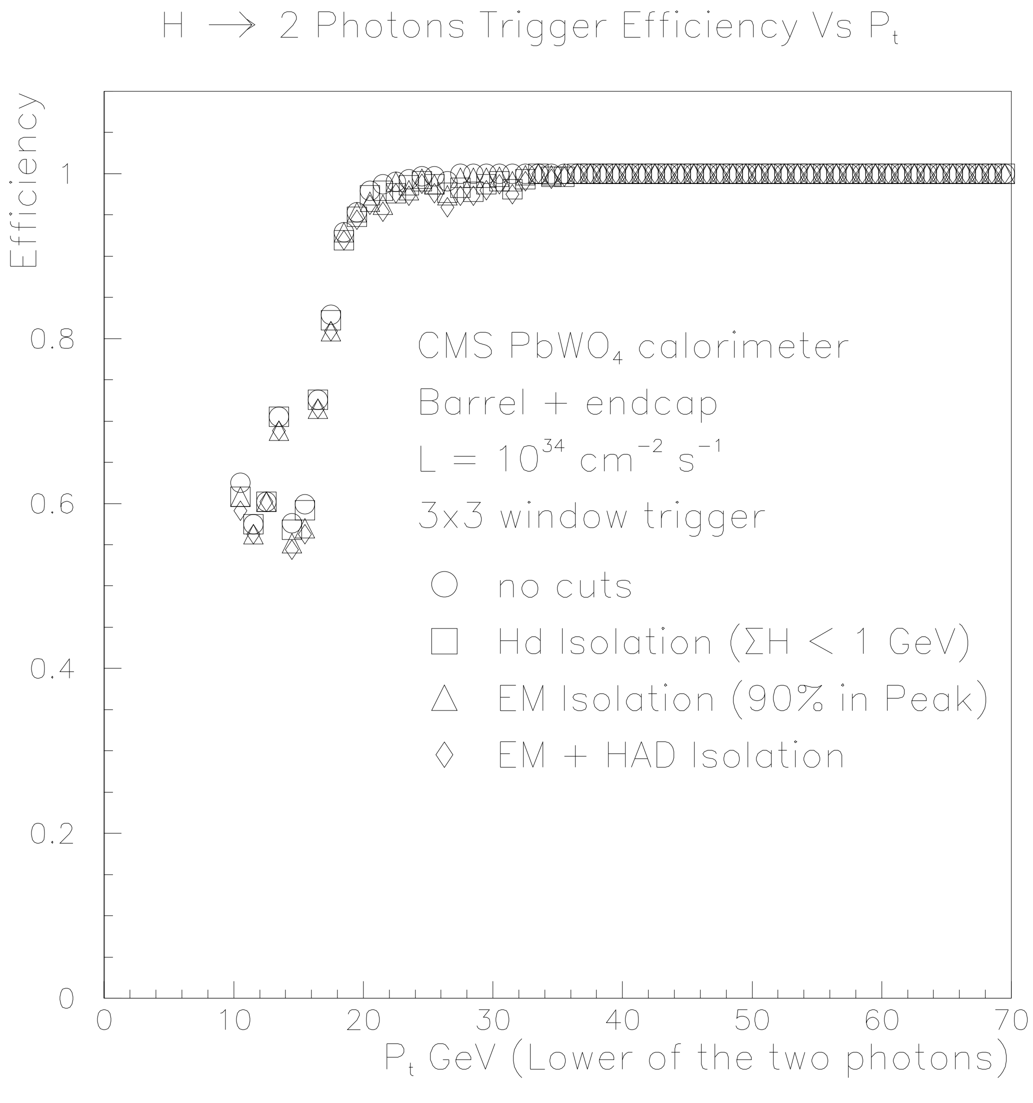

Figure 19: Peak finding algorithm efficiency for triggering on two photons from Higgs ($M_H = 80$ GeV) decay.

Algorithm	Electron/photoon E_t Cutoff (GeV)	Rate (kHz)	95% p_t Thresh (GeV)	Tot Eff %	Dielectron/diphoton E_t Cutoff (GeV)	Rate (kHz)	95% p_t Thresh (GeV)	Tot Eff %
Sliding	25	11.5			12.5	5.9		
Window	30	5.7	40	99.1	15.0	3.1	21	99.9
Had Iso	35	3.0			17.5	1.1		
Sliding	25	9.6			12.5	3.9		
Window	30	4.7	40	97.8	15.0	2.1	21	99.9
EM + Had Iso	35	2.4			17.5	0.7		
Peak	25	10.5			12.5	11.		
Finding	30	5.6	39	98.9	15.0	5.7	19	99.6
Had Iso	35	2.8			17.5	2.7		
Peak	25	8.1			12.5	5.2		
Finding	30	4.5	39	98.2	15.0	2.3	20	98.9
EM + Had Iso	35	2.2			17.5	1.0		

Table 4: Summary of rate and efficiency for sliding window and peak finding electron/photon trigger algorithms for the nominal LHC design luminosity of $10^{34}\text{cm}^{-2}\text{s}^{-1}$. The 95% p_t efficiency column indicates the p_t above which the trigger efficiency is 95%. The total efficiency column lists the total efficiency for a p_t 10 GeV above the set E_t cutoff.

7 Jet trigger rates and efficiency

The jet trigger is important in the study of QCD physics at the LHC. Since lower p_t jet triggers will be produced profusely at the LHC, the physics requirements are not as stringent as those for electrons and photons. The jet trigger thresholds need to be large enough to keep the rate below a few kHz, yet one should be able to provide a highly efficient trigger to study QCD physics that has sufficient overlap with the Tevatron data. In addition, several prescaled jet triggers must be available with thresholds below the nominal full acceptance unprescaled jet trigger. Finally, the low-p_t jet trigger efficiency must have a sufficiently sharp turn-on curve to be useful in combination with other electron/photon, muon or jet triggers.

In order to achieve the best efficiency with the lowest rate, we have studied the effect of the size of the jet trigger tower summation region. The jet trigger rates and efficiencies for various regions of summation are plotted in Figures 20, 21 and 22. The jet trigger efficiency is plotted versus the p_t of the parton before fragmentation. The transverse energy sums in a $0.35\eta \times 0.35\phi$ (4 x 4 trigger towers) region or overlapping regions of $0.7\eta \times 0.7\phi$ (i.e. two grids of 8 x 8 trigger towers covering $0.7\eta \times 0.7\phi$ offset from each other by 0.35η and 0.35ϕ) provide sufficient performance. For example, a 1 kHz rate jet trigger can be achieved with an E_t cutoff of 141 GeV for a $0.35\eta \times 0.35\phi$ trigger, or 168 GeV for a overlapping $0.7\eta \times 0.7\phi$ trigger. These cutoffs yield parton p_t thresholds, with 95% efficiency, of 350 and 300 GeV respectively.

Some SUSY particle searches require triggers with multiple jets. These channels place a constraint on the jet trigger summation region size because too large a region might cause suppression of multi-jet triggers. Multi-jet triggers in association with a lepton may be useful in increasing the top quark event yield. In order to understand the efficiency of jet identification for such combination triggers the efficiency for jets is plotted for 100 kHz rate in figure 22. While the efficiency curves for the $0.35\eta \times 0.35\phi$ region and overlapping regions of $0.7\eta \times 0.7\phi$ appear adequate, the performance must be studied for specific processes and combinations of triggers. These studies are underway.

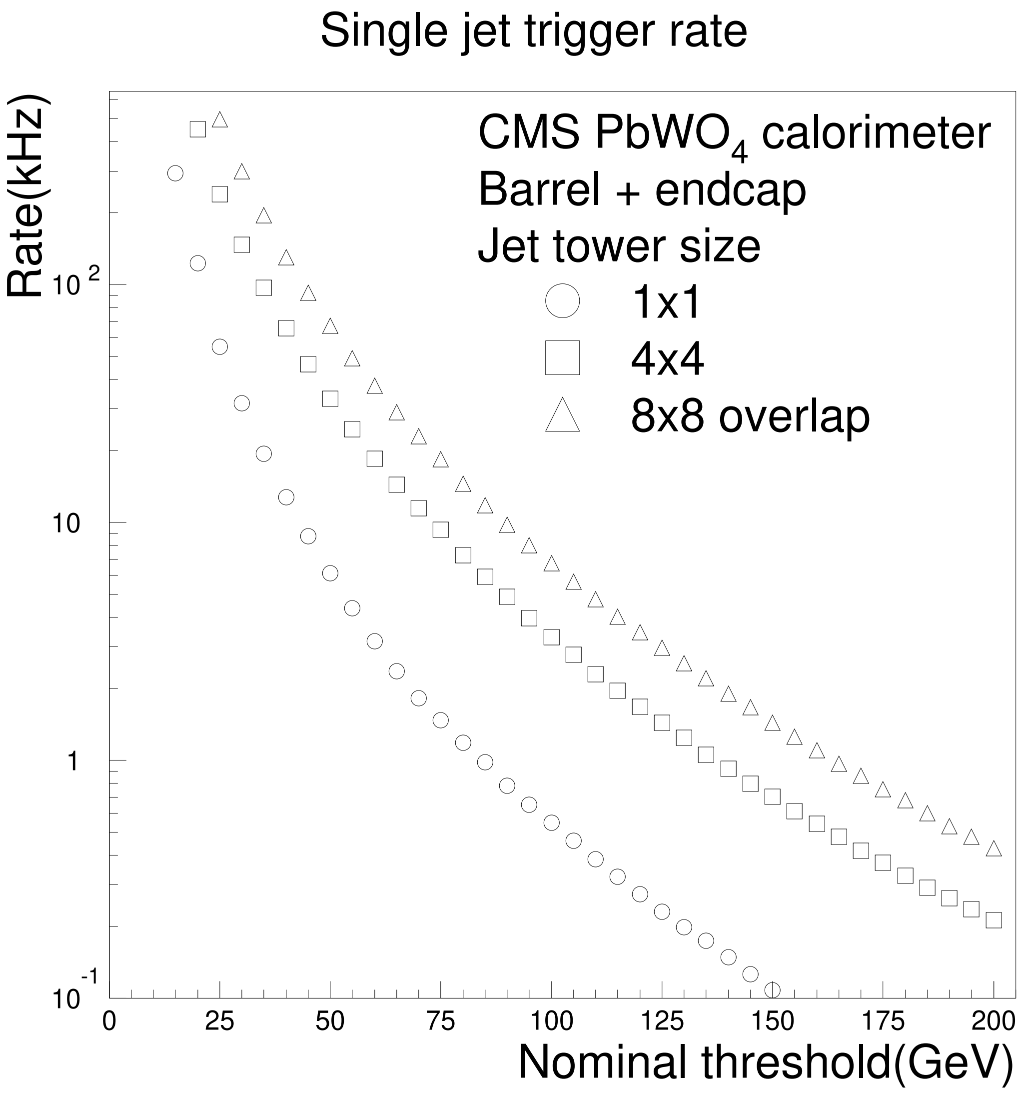

Figure 20: Jet trigger rates using various tower region sums are plotted versus the E_t deposited in the calorimeter region. The rate includes only barrel and endcap calorimeters, i.e. $|\eta| < 2.6$.

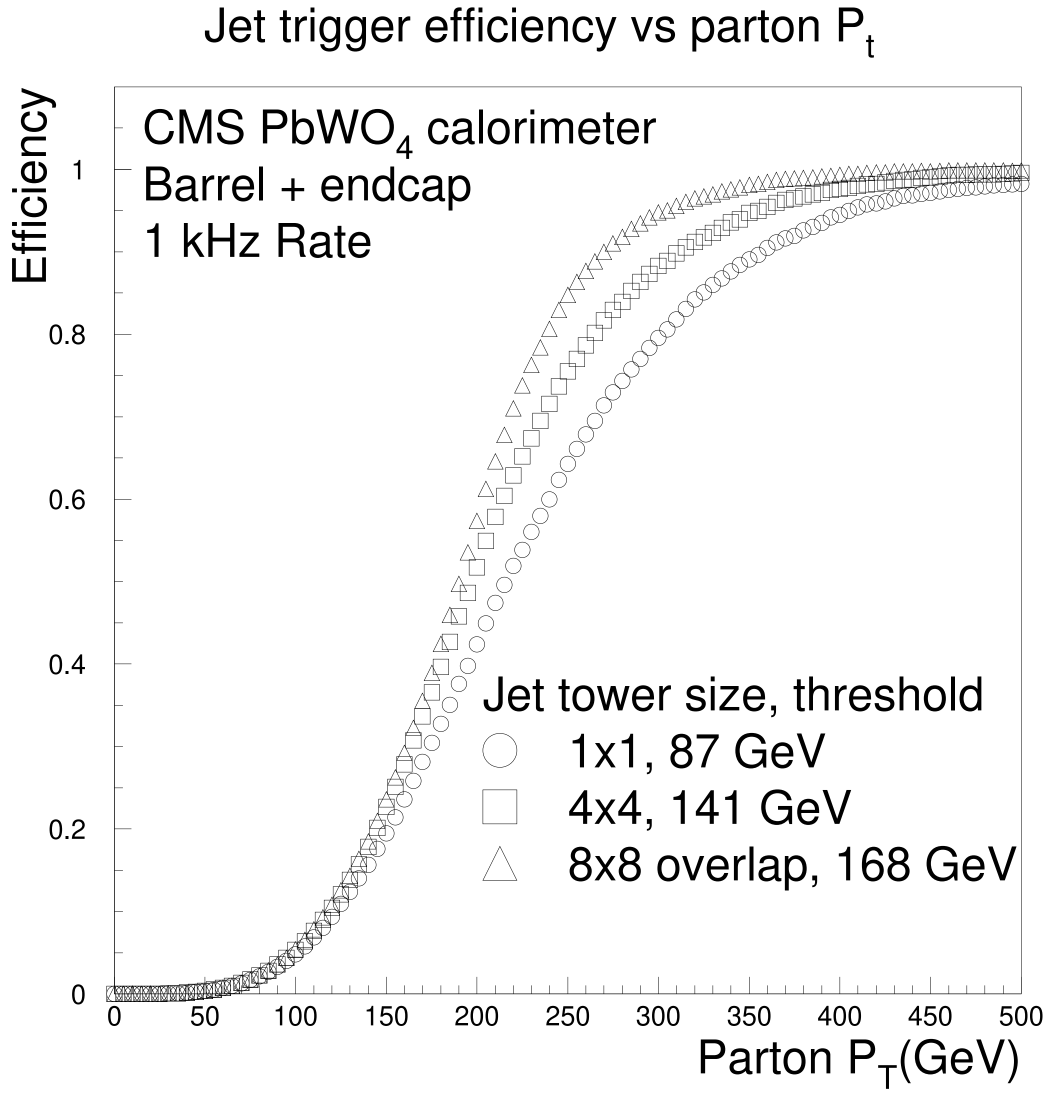

Figure 21: Efficiency of jet trigger for various tower region sums is plotted versus the parton p_t. The thresholds for different tower region sums are set such that rate from them is always 1 kHz.

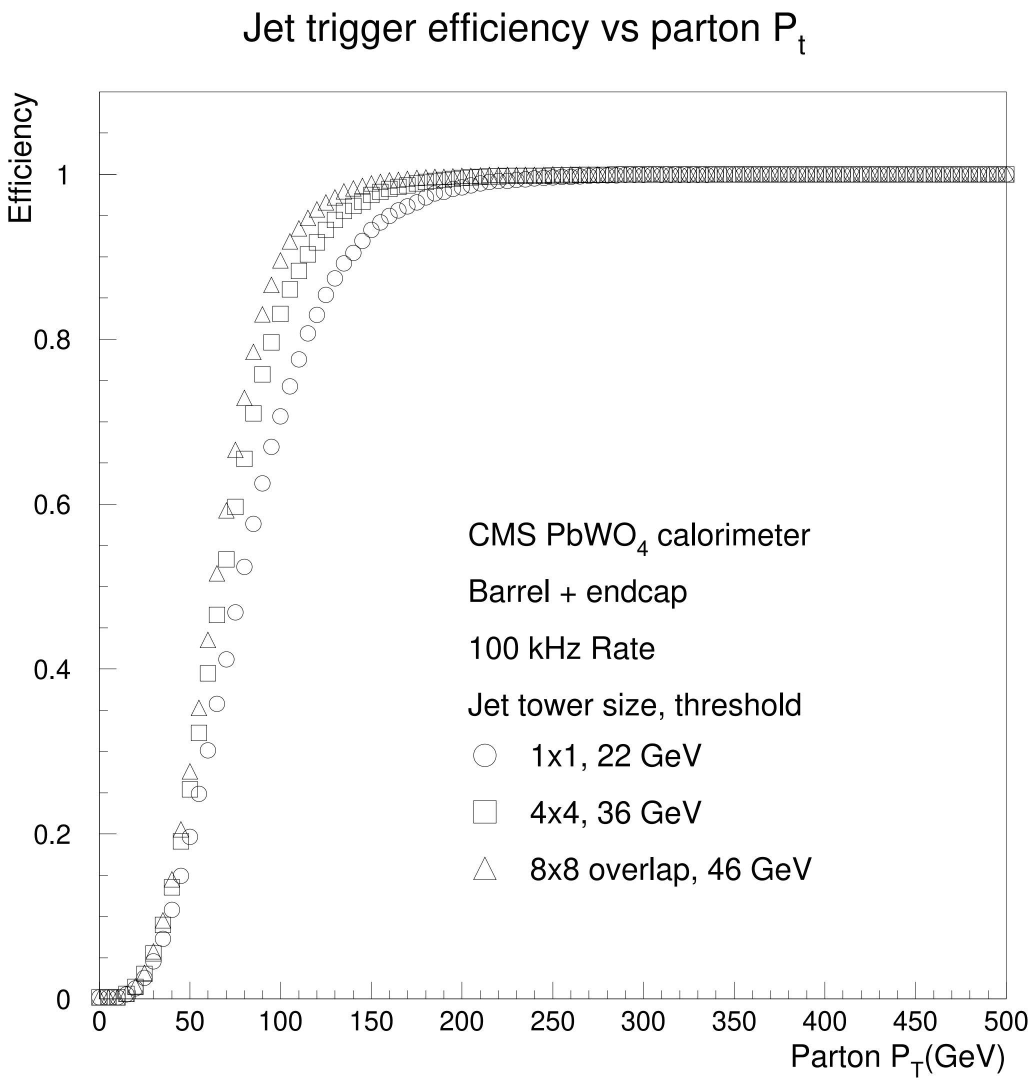

Figure 22: Efficiency of jet trigger for various tower region sums is plotted versus the parton p_t. The thresholds for different tower region sums are set such that rate from them is always 100 kHz.

8 Conclusions

We have used a simulation of the CMS detector to show that the rate and efficiency performance of both sliding window and peak finding algorithms for the single and di- electron/photon triggers, as well as the sliding window jet trigger algorithm are well within the requirements of the CMS detector. This simulation is based on a realistic CMS calorimeter trigger conceptual design and the CMS $PbWO_4$ calorimeter. We have simulated Drell-Yan W, and top decay electrons as well as Higgs decays to 2 photons.

We find that the use of HAD isolation for the electron/photon triggers provides good rejection without a loss in efficiency for both the barrel and endcap calorimeter, and satisfies the CMS rate requirements. The performance of the sliding window and peak finding algorithms are identical within the uncertainties of the simulation and the optimization of the algorithm parameters. For both algorithms, most of the rate reduction for the electron/photon triggers is provided by the HAD isolation criteria. The EM isolation criterion does not provide a substantial additional reduction in rate if high efficiency is maintained. At low luminosity, the sliding window algorithm can be used with the H/E cut alone (i.e. without the full transverse HAD isolation) for top and bottom physics. At higher E_t, the HAD isolation and eventually, the H/E cuts can be removed to ensure full efficiency for the highest p_t electrons. Finally, we have shown that jet sum regions composed of 4 x 4 or overlapping 8 x 8 trigger tower regions yield sufficient performance for the jet trigger.

References

[1] J. Lackey et al., *CMS Level 1 Calorimeter Trigger Design*, CMS TN/94-284.

[2] CMS, The Compact Muon Solenoid, Letter of Intent, CERN/LHCC 92-3, 1 October 1992; Status Report and Milestones, CERN/LHCC 93-48, 15 October 1993.

[3] J. Varela and P. Busson, CMS TN/94-219.

[4] J. Varela, *Proceedings of CMS trigger meeting*, Bad Aussee, Austria, 1994.

[5] S. Dasu et al., *CMS level 1 Calorimeter Trigger*, Proc. of the Int. Conf. on Computing in HEP, San Fransisco, CA, 1994.

[6] S. Dasu et al., *The level 1 Calorimeter Trigger for the CMS detector at LHC* Proc. of the Int. Conf. on Calorimetry in HEP, Upton, NY, 1994.

[7] Particle Data Group, Phys. Rev. D50 (1994) 1173.

[8] Bock et al., NIM 186 (1981) 533.

[9] Binon et al., NIM 206 (1983) 373.